



AMERICAN METEOROLOGICAL SOCIETY

Journal of Physical Oceanography

EARLY ONLINE RELEASE

This is a preliminary PDF of the author-produced manuscript that has been peer-reviewed and accepted for publication. Since it is being posted so soon after acceptance, it has not yet been copyedited, formatted, or processed by AMS Publications. This preliminary version of the manuscript may be downloaded, distributed, and cited, but please be aware that there will be visual differences and possibly some content differences between this version and the final published version.

The DOI for this manuscript is doi: 10.1175/JPO-D-13-047.1

The final published version of this manuscript will replace the preliminary version at the above DOI once it is available.

If you would like to cite this EOR in a separate work, please use the following full citation:

Durgadoo, J., B. Loveday, C. Reason, P. Penven, and A. Biastoch, 2013: Agulhas Leakage Predominantly Responds to the Southern Hemisphere Westerlies. *J. Phys. Oceanogr.* doi:10.1175/JPO-D-13-047.1, in press.



1 **Agulhas leakage predominantly responds to the**
2 **Southern Hemisphere westerlies**

3
4 Jonathan V. Durgadoo¹

5 *GEOMAR Helmholtz Centre for Ocean Research Kiel, Germany*
6

7
8 Benjamin R. Loveday

9 *Department of Oceanography, University of Cape Town, South Africa*
10

11
12 Chris J.C. Reason

13 *Department of Oceanography, University of Cape Town, South Africa*
14

15
16 Pierrick Penven

17 *LMI ICEMASA, LPO, UMR 6523 (CNRS, IFREMER, IRD, UBO), France*
18

19
20 Arne Biastoch

21 *GEOMAR Helmholtz Centre for Ocean Research Kiel, Germany*
22
23
24

¹ *Corresponding author address:* Jonathan Durgadoo, GEOMAR Helmholtz Centre for Ocean Research
Kiel, 24105, Germany.
E-mail: jdurgadoo@gmail.com

25
26
27
28
29
30
31
32
33
34
35
36
37
38
39
40
41
42
43
44
45
46

Abstract

The Agulhas Current plays a crucial role in the thermohaline circulation through its leakage into the South Atlantic. Under both past and present climates, the trade winds and westerlies could have the ability to modulate the amount of Indian-Atlantic inflow. Compelling arguments have been put forward suggesting that trade winds alone have little impact on the magnitude of Agulhas leakage. Here, employing three ocean models for robust analysis – a global coarse resolution, a regional eddy-permitting and a nested high-resolution eddy-resolving configuration – and systematically altering the position and intensity of the westerly wind belt in a series of sensitivity experiments, it is shown that the westerlies, in particular their intensity, control the leakage. Leakage responds proportionally to the westerlies intensity up to a certain point. Beyond this, through the adjustment of the large-scale circulation, energetic interactions occur between the Agulhas Return Current and the Antarctic Circumpolar Current that result in a state where leakage no longer increases. This adjustment takes place within 1 to 2 decades. Contrary to previous assertions, our results further show that an equatorward (poleward) shift in westerlies increases (decreases) leakage. This occurs due to the redistribution of momentum input by the winds. It is concluded that the reported present-day leakage increase could therefore reflect an unadjusted oceanic response mainly to the strengthening westerlies over the last few decades.

47 1. Introduction

48 The climatically relevant component of the Agulhas Current system is arguably its inflow
49 into the South Atlantic (de Ruijter et al. 1999). One of the unique features of this western
50 boundary current system is that it redistributes heat and salt not only poleward but also
51 equatorward in the form of Agulhas leakage (Fig. 1). The equatorward injection of warm
52 salty thermocline waters into the Atlantic forms a major part of the return flow towards
53 the North Atlantic, where, through active air-sea interactions at high latitudes, deep
54 waters are formed (Gordon 1986; Gordon et al. 1992; Cunningham and Marsh 2010). In
55 this way, the Agulhas system is considered to be important for global climate (Beal et al.
56 2011) and as a result, the variability of Agulhas leakage on all timescales is of particular
57 interest. In the past, some evidence for leakage reduction during glacial times (Peeters et
58 al. 2004), possibly modulated by a northward migration of the subtropical front south of
59 Africa (Bard and Rickaby 2009), has been inferred from sediment records. At glacial
60 terminations, increase in leakage has been further linked with the recovery of the Atlantic
61 thermohaline circulation (Knorr and Lohmann 2003). Under the current (and future)
62 warming climate, model studies suggest an increasing trend in Agulhas leakage (Biaستoch
63 et al. 2009a; Rouault et al. 2009) that result in an overall salinification of the South
64 Atlantic (Biaستoch and Böning 2013). The effectiveness of this significant exchange south
65 of Africa for the most part is thought to be linked in one way or another to the wind
66 patterns of the Southern Hemisphere (Biaستoch et al. 2009a; Rouault et al. 2009).

67 The Agulhas system is sandwiched between two major wind belts, namely the
68 southeast trades, between the Equator and about 30°S, and the westerlies, over roughly
69 30° – 60°S. With the average latitudinal range of the positive wind stress curl region in

70 the Indian Ocean extending beyond the termination of the African continent near 34°S
71 (Marshall and Plumb 2007), the Agulhas Current leaves the continental slope as a free-
72 jet. An interplay between its large inertia and the position of the zero wind stress curl
73 (maximum westerlies) leads to its retroflection (Ou and de Ruijter 1986), a process which
74 also determines the amount of leakage into the Atlantic (de Ruijter et al. 1999; Pichevin
75 et al. 1999; Dijkstra and de Ruijter 2001). Therefore, the variability of Agulhas leakage
76 on all timescales is expected to be connected to the trades and/or westerlies strength
77 and/or position.

78 The trade winds are largely responsible for the inertia of the Agulhas Current.
79 Rouault et al. (2009) and van Sebille et al. (2009) (who used the same model as Biastoch
80 et al. (2009a)) found the contemporary increase in leakage to be linked with the upstream
81 strength of the Agulhas Current. Within their range of model observations, they however
82 disagreed on the sign of the relationship; Rouault et al. (2009) claimed an increase in
83 leakage caused by increase in Agulhas Current, while van Sebille et al. (2009) argued for
84 a decrease in the upstream inertia that leads to an increase in leakage. Both of these
85 studies implied that the trade winds influence leakage magnitude. In a series of realistic
86 global and regional ocean/sea-ice models, Loveday et al. (submitted) showed that the
87 sensitivity of Agulhas leakage to the Agulhas Current transport decreases with increasing
88 horizontal resolution. In the eddy-resolving simulations, large changes in the upstream
89 transport of the Agulhas Current had almost no effect on the magnitude of the leakage.
90 Even though a stronger Agulhas transport did cause the Agulhas Current to break from
91 the shelf further upstream (Ou and de Ruijter 1986), the inertial jet always proceeded
92 south-westward. As a result, despite large localized changes in both mean and eddy

93 kinetic energy, the annual mean retroflection position remained stable, consistent with
94 observed present-day (Dencausse et al. 2010) and reconstructed past (Franzese et al.
95 2009) measurements, and Agulhas leakage is unaffected. The increase in kinetic energy
96 possibly leads to a recently described turbulent retroflection regime (Le Bars et al. 2012)
97 where leakage is no longer dependent on the incoming transport.

98 Given this apparent decoupling between Agulhas leakage and trade winds, in this
99 study we explore the possible dependency of leakage on the Southern Hemisphere
100 westerlies. We systematically alter the position and magnitude of the westerly wind belt
101 within three model configurations similar to those used by Biastoch et al. (2009a) and
102 van Sebille et al. (2009) (half-degree global, with and without a tenth-degree nest) and
103 Rouault et al. (2009) (quarter-degree regional) in order to achieve robust results. The
104 strategy we employ generally follows the works of Oke and England (2004), Sijp and
105 England (2008, 2009) and Biastoch and Böning (2013). The models are all forced by the
106 same atmospheric data and consistent diagnostics are derived. In so-doing, we aim to dis-
107 entangle the relationship between the magnitude of Agulhas leakage and the westerlies
108 location and strength.

109 Following a description of the models and of our experiment strategy in section 2
110 we explore the equilibrium (section 3) and transient (section 4) leakage response to
111 westerlies change. In section 5 we seek a mechanism explaining the results and then
112 discuss the implications in section 6 before summarizing our main findings in section 7.

113 2. Model configurations and Experiment Strategy

114 The three models employed in this study are ORCA05, INALT01 and AGIO. The first
115 two, based on the ocean/sea-ice Nucleus for European Modeling of the Ocean code

116 (NEMO v3.1.1, Madec (2008)) and developed under the DRAKKAR framework (The
117 DRAKKAR Group 2007) are global models and will be described first. AGIO,
118 summarized thereafter, is a regional model based on the Regional Ocean Modeling
119 System (ROMS, Shchepetkin and McWilliams (2005)) and is described thoroughly in
120 Loveday et al. (submitted). Similar configurations of these models were used by Biastoch
121 et al. (2009a), Rouault et al. (2009) and van Sebille et al. (2009) but with different setups
122 and forcing fields which we hypothesize have led to their conflicting results. To assess
123 this, we performed all experiments under same atmospheric forcing with as much
124 coherence and conformity as possible.

125 *a. ORCA05 and INALT01*

126 Both ORCA05 (coarse resolution configuration) and INALT01 (nested configuration)
127 follow an ORCA setup (Madec and Imbard 1996; Barnier et al. 2006). In this setup a tri-
128 polar horizontal grid is used and south of 20°N, the grid is Mercator-type. Variables are
129 staggered following an Arakawa-C arrangement. In the vertical, the model uses z-
130 coordinates with a total of 46 levels (10 levels in the top 100 m and a maximum of 250 m
131 resolution at depth). In order to enhance representation of flow near bottom topography,
132 the deepest grid box is allowed to be partially filled (Barnier et al. 2006) in addition to a
133 non-linear bottom friction (Tréguier 1992). A free-slip lateral momentum boundary
134 condition is used. The treatment of tracers is implemented using a Laplacian operator for
135 the lateral diffusion and the Total Variance Dissipation (Zalesak 1979) scheme for
136 advection. Lateral diffusion on momentum uses a bi-Laplacian operator with a vector
137 form advection scheme that conserves energy and enstrophy (Arakawa and Hsu 1990).

138 Sub-grid scale vertical mixing is calculated explicitly through the turbulent eddy kinetic
139 dependent diffusion scheme (Blanke and Delecluse 1993).

140 ORCA05, with half-degree nominal horizontal resolution, which in the Agulhas
141 region is ~45 km, is an established configuration successfully reproducing the large-scale
142 global circulation (Biaستoch et al. 2008a). INALT01 consists of a base global model (that
143 is identical in configuration to ORCA05) and a nest embedded within between 70°W –
144 70°E and 50°S – 8°N (Fig. 1). The nest refines the horizontal model grid over the
145 Agulhas Current system and South Atlantic 5-folds to a tenth-degree (~9 km over the
146 Agulhas region). This also implies a 4-fold time-stepping refinement from 36 (base) to 9
147 (nest) minutes. Bathymetry within the nest region is interpolated from ETOPO2¹.

148 The horizontal refinement is achieved by adopting the AGRIF (Debreu and Blayo
149 2008) approach whereby both model grids are coupled in a 2-way mode at every base
150 model time-step to provide the nest with open boundary conditions from the base but also
151 enabling the mesoscale dynamics of the nest to permeate into the base. For this reason,
152 neither INALT01's base nor ORCA05 have parameterized mesoscale eddies, a practice
153 that is usually common for models of such resolution class. Eddy parameterization, such
154 as the Gent and McWilliams (1990) scheme, typically mimics the impact of eddies on
155 tracer fluxes as isopycnal diffusion and eddy advection. This has an overall effect of
156 reducing isopycnal steepness. Such parameterization is believed to dampen the influence
157 of the mesoscale dynamics of the nest onto the base. ORCA05 was also run without eddy
158 parameterization in order to allow consistent comparison between both models.

159 INALT01 is an update of AG01 (Biaستoch et al. 2009b), the latter has been
160 demonstrated to represent the dynamics of the Agulhas Current and its large-scale impact

¹ <http://www.ngdc.noaa.gov/mgg/global/relief/ETOPO2/ETOPO2v2-2006/ETOPO2v2g/>

161 successfully (Biaostoch et al. 2008b,c, 2009a,b; van Sebille et al. 2009). With its wider
162 high-resolution domain encompassing the South Atlantic basin as well as the tropical
163 Atlantic, INALT01 better lends itself to the investigation of the hypothesized impact of
164 Agulhas leakage on the Atlantic heat, freshwater and momentum balances. In addition,
165 the advective pathways between the Agulhas system and the North Atlantic can be
166 further explored. The new configuration simulates successfully two major western
167 boundary currents of the Southern Hemisphere.

168 Prescribing appropriate atmospheric forcing is crucial for ocean modeling. The
169 CORE (v2b, Large and Yeager (2009)) project provides the necessary coherent and
170 globally balanced dataset to drive the model. Through bulk formulation, 6-hourly air-sea
171 fluxes of heat, freshwater and momentum, daily short- and long-wave radiation and
172 monthly rain and snow, are used in conjunction with surface ocean temperatures and
173 velocities, which effectively allow some feedback between ocean and atmosphere. For
174 this study, both climatologically and inter-annually varying CORE fields were used.

175 Ocean-only models often exhibit drifts in properties. In order to constrict such
176 artificial drifts within ORCA05 and INALT01, a 10 % precipitation reduction (which
177 falls within the CORE dataset uncertainty range) north of 55°N is implemented in
178 addition to a sea surface salinity restoring over the top 50 m with a timescale of 8.3 years.
179 This “very weak” salt flux damping is capped at $0.5 \text{ kg m}^{-1} \text{ s}^{-1}$ to prevent regions of
180 strong gradients from being excessively damped.

181 Initializing the thermohaline fields with a combined dataset from Levitus World
182 Ocean Atlas 1998¹ and Polar Science Centre Hydrographic Climatology (Steele et al.
183 2001), and starting from rest, ORCA05 is allowed to spin-up for 20 years forced with

¹ <http://www.esrl.noaa.gov/psd/>

184 inter-annually (1978-1997) varying CORE fields. This strategy promotes a stable Atlantic
185 meridional overturning circulation with a reasonable magnitude of ~ 18 Sv (Cunningham
186 and Marsh 2010) which, in the previous version (AG01), was ~ 10 Sv (Biaostoch et al.
187 2008b). Dynamic equilibrium is reached within the 20 years of spin-up (Fig. 2) and this
188 output is then used to warm-start the experiments outlined in Section 2c.

189 *b. AGIO*

190 The AGIO configuration (Loveday et al. submitted) is a quarter-degree resolution eddy-
191 permitting implementation of ROMS (Shchepetkin and McWilliams 2005), constructed
192 using ROMSTOOLS (Penven et al. 2008). The domain, which extends from 29°W to
193 115°E and 48°S to 7°N on a Mercator grid, spans the Indian and South East Atlantic
194 Ocean basins. AGIO is an extension of the SAfE configuration (Penven et al. 2006)
195 which was used by Rouault et al. (2009). The average grid spacing over the southern
196 Agulhas region is ~ 23 km. The vertical resolution in AGIO is described by 32 σ -
197 coordinate levels following the GEBCO1¹ derived bathymetry and stretched towards the
198 surface. The regional bathymetry is selectively smoothed to reduce pressure gradient
199 errors (Haidvogel and Beckmann 1999). Higher order numerics and a third-order,
200 upstream-biased advection scheme reduce dispersion, allowing steep density gradients to
201 be preserved, and enhancing precision for a given resolution (Shchepetkin and
202 McWilliams 1998). The splitting of diffusion and advection via the RSUP3 scheme
203 minimizes spurious diapycnal mixing (Marchesiello et al. 2009). Western boundary
204 currents are selectively damped via a parameterization of horizontal viscosity
205 (Smagorinsky 1963) and sub-grid scale vertical mixing follows a non-local K-Profile

¹ http://www.gebco.net/data_and_products/gridded_bathymetry_data/

206 parameterization (Large et al. 1994). The lateral viscosity and diffusion are zero in the
207 domain interior and increase to $1000 \text{ m}^2 \text{ s}^{-1}$ in the sponge layer within ~ 200 km from the
208 domain boundaries. Prognostic variables are connected to the external conditions by an
209 active radiation scheme (Marchesiello et al. 2001). Lateral boundary conditions for all
210 AGIO experiments are derived from the climatological-monthly-mean ORCA05
211 reference experiment, and variability associated with the Antarctic Circumpolar Current
212 is thereby excluded. AGIO is initialized with outputs from the ORCA05 20-year spin-up.

213 *c. Experiment Design and Application*

214 The experiments we performed are to some extent similar to those presented by Oke and
215 England (2004) and Sijp and England (2008, 2009). Anomalies applied to the present-day
216 wind patterns (Fig. 3a) were designed to mimic different states in westerlies regime;
217 equatorward and poleward shifts of $\pm 2^\circ$ and $\pm 4^\circ$ of latitude (Fig. 3b) and intensity
218 changes of $\pm 20\%$ and $\pm 40\%$ (Fig. 3c). The values chosen roughly span the range of
219 observed (Swart and Fyfe 2012), 21st century projected (Fyfe and Saenko 2006; Fyfe et
220 al. 2007) as well as past (Hodgson and Sime 2010) changes in westerly winds. These
221 anomalies have a smooth and quasi-sinusoidal shape to avoid any sharp changes or
222 disruptions in the general wind stress curl pattern (that would alter the general pattern of
223 the circulation). Additional design considerations were: (i) Changes to the westerlies
224 were limited to south of 35°S such that no changes are applied to the latitudes that would
225 influence the inertia of the western boundary current; (ii) Shifts were constructed based
226 on the latitudinal location of the maximum wind stress and the total energy input kept
227 constant; (iii) The meridional wind stress component were unchanged. These
228 considerations imposed limits to the extent the westerlies could be altered.

229 The resulting anomalies were reproduced onto the respective model-grids. Out of
230 the 8 anomalies (Fig. 3b, c), a total of 15 anomaly fields were produced (Table 1). For
231 some anomalies, in particular the SHW+40% anomaly (westerlies intensity increase by
232 40%), in addition to changing the intensity of the wind stress, we also altered the region
233 over which these anomalies were applied (Fig. 4). These geographical decompositions
234 attempt to determine the influence the Antarctic Circumpolar Current may have on the
235 Agulhas system. For these cases, additional smoothing was applied along the boundaries.
236 The 2-dimensional wind anomaly fields were added after calculation of the wind stress.
237 Thus, the application influences the momentum and not the buoyancy input to the
238 ocean/sea-ice. This strategy follows Biastoch and Böning (2013) who performed a similar
239 experiment within AG01.

240 All three models, sharing the same 20-year spin-up history, were forced under
241 background CORE climatological forcing (Large and Yeager 2009). Fig. 2 exemplifies
242 the adjustment of the models. A relatively fast adjustment in volume integrated kinetic
243 energy to changes in resolution and forcing (application of anomaly) is noted. The
244 reference experiments were integrated for 30 years before application of the anomalies.
245 At first they were applied with a linear ramp-up over one year (model year 31) and
246 subsequently in full. Reference and sensitivity simulations ran parallel from model year
247 31. After two decades of parallel integration, analysis for all simulations was performed
248 for a common period of 10 years (model years 51 – 60). The increasing kinetic energy
249 after model year 45 in the global models for the SHW+40% examples shown in Fig. 2
250 reflects the transient response of the Agulhas system to the enhanced winds. This is
251 discussed in Section 4. Some selected experiments were extended, as outlined in Table 1.

252 The models were additionally integrated under inter-annually varying surface forcing,
253 providing 6 decades (1948 – 2007) of hind-cast simulations.

254 *d. Model Validations*

255 Given the dominance of mesoscale variability, direct one-to-one comparison with
256 features observed during oceanographic expeditions cannot be expected, even though a
257 high-frequency, inter-annually varying forcing is used. However, time-mean properties
258 and statistical representation of the variability ought to be comparable. ORCA05 is an
259 established configuration of NEMO (Biaستoch et al. 2008a). Both AGIO and INALT01
260 are updates of previously thoroughly tested configurations; SAfE (Penven et al. 2006)
261 and AG01 (Biaستoch et al. 2008b,c,2009b; van Sebille et al. 2009,2010) respectively.
262 Within ORCA05, the Agulhas Current is represented by a continuous flow that begins in
263 the Northern Mozambique Channel with the only source of variability originating south
264 of Madagascar. The current retroflects and occasionally produces some large unrealistic
265 rings. In contrast, within AGIO and INALT01, where the first baroclinic Rossby radius of
266 deformation is resolved (20 – 50 km in this region, Chelton et al. (1998)), a broad
267 spectrum of mesoscale activity is observed in the known source regions of the Agulhas
268 Current as well as a more realistic representation of the diverse range of features typically
269 found in the Cape Cauldron, namely Agulhas Rings, Cyclones and filaments among
270 others (Boebel et al. 2003). Fig. 5 portrays the models reproduction of the mean
271 circulation as well as the mesoscale variability of the Agulhas system compared to that
272 observed from satellite altimetry (Fig. 5a). The mean circulation is successfully
273 represented by all three models; the details of the variability do however differ.

274 *e. Assessing Agulhas leakage*

275 Measuring Agulhas leakage is no simple task. Being highly intermittent, leakage occurs
276 predominantly through Agulhas rings. However, other features such as cyclones and
277 filaments also contribute to the Indian-Atlantic transport. Therefore, direct quantification
278 of Agulhas rings crossing the Cape Basin would likely underestimate leakage magnitude
279 (de Ruijter et al. 1999), while full-depth Eulerian measurements would over estimate it.
280 Attempts at estimating leakage using optimized Eulerian methods have been made (van
281 Sebille et al. 2010) but the skills of such methods have not been tested across models
282 with different horizontal and vertical resolutions. From float and drifter observations,
283 Richardson (2007) estimated leakage to be at about 15 Sv.

284 Here, we estimated annual values of leakage using a Lagrangian method
285 following the works of Speich et al (2001), Biastoch et al. (2008b, 2009a) and van Sebille
286 et al. (2009). Water parcels were released every 5 days for one year over the full-depth of
287 the poleward-flowing Agulhas Current across a zonal 300 km long segment at 32°S. Each
288 parcel had a defined transport of max. 0.1 Sv and the total number of parcels released
289 were representative of the 5-daily magnitude of the Agulhas Current. The parcels were
290 then advected using the model's velocity fields for a total period of five years and
291 aggregated across predefined sections. The integration period optimally allowed 98 % of
292 the parcels to exit the domain shown in Fig. 5d. Agulhas leakage is defined as that
293 portion of the Agulhas Current exiting the domain through the Good-Hope section
294 (Ansorge et al. 2005) in the Cape Basin (Fig. 5b). The advantage of this method is that it
295 can be applied to all three models without the need for additional model-specific
296 redefinitions, allowing direct inter-model comparisons. The southward transport of the

297 Agulhas Current at 32°S for model years 51 – 60 of the three REF experiments are $71.9 \pm$
298 0.7 , 72.9 ± 3.1 and 64.6 ± 2.6 Sv for ORCA05, AGIO and INALT01 respectively. The
299 corresponding reference leakage values for the same period are 31.9 ± 1.5 , 31.5 ± 1.4 and
300 16.6 ± 1.7 Sv respectively. It is clear that leakage is markedly influenced by the regional
301 mesoscale (Biastoch et al. 2008c).

302 3. Agulhas leakage equilibrium response

303 Owing to the different reference values of Agulhas leakage in the three models, we adopt
304 the percentage change with respect to reference as a measure of leakage response. This
305 places all reference values at the origin. The 10-year-mean (model years 51 – 60) leakage
306 response to changes in position (Fig. 6a) and intensity (Fig. 6b) of the westerlies display
307 three clear patterns. Firstly, within the global models, an equatorward (poleward) shift in
308 westerlies produces an increase (decrease) in leakage. Note that AGIO's southern
309 boundary at 48°S makes shift experiments not sensible. Secondly, increasing westerlies
310 intensity generally produces more leakage but the relationship is not completely linear.
311 Finally, leakage responds preferentially, and the magnitude of that response is more
312 pronounced when changes are applied to the westerlies intensity than shifts. For this
313 reason, we will concentrate on the intensity cases and return to the shifts towards the end.
314 Interestingly, for strong wind stress in Fig. 6b, both global models simulate very little
315 leakage change and even reduction compared to the reference values. Conversely, a 20 %
316 and 40 % reduction in wind stress produces approximately the same amount of leakage
317 decrease. Consistent with Le Bars et al. (2012), there appears to be a threshold in leakage
318 response to increased westerlies.

319 In order to investigate the reason for this threshold, we focus on two extreme
320 intensity cases, SHW \pm 40% within ORCA05. The Agulhas system, forming part of the
321 subtropical gyres of the south Atlantic and south Indian Oceans (Ridgway and Dunn
322 2007) and bounded by the Antarctic Circumpolar Current, potentially could be influenced
323 by numerous external factors. In an attempt to therefore distinguish between local and
324 large-scale wind impact on leakage, a geographical decomposition of the SHW \pm 40%
325 experiments was performed (Fig. 4a-c). We favored the use of the coarse resolution
326 ORCA05 model since it is computationally less demanding. The response shown in Fig.
327 6c reveals that the overall leakage response consists of the direct influence of the
328 westerlies acting locally (over the Agulhas Retroflexion and Cape Basin region) on the
329 magnitude of the leakage and on the indirect influence of the winds via the adjacent
330 currents. INALT01, the configuration that mimics the known complexity of the Agulhas
331 system with the highest degree of semblance, reproduces the general behavior in leakage.
332 Leakage response within INALT01-SHW+40% with LOCAL decomposition shows that,
333 despite the overestimation of absolute leakage values within the coarse resolution model,
334 the change in leakage is consistent. The decompositions further indicate that the threshold
335 in leakage change originates from the large-scale circulation, within which the Agulhas
336 system is embedded.

337 This hypothesis is tested by employing the regional model, AGIO, whose domain
338 excludes much of the large-scale circulation (Loveday et al. submitted). The global ocean
339 influences this regional model through lateral boundary conditions derived from
340 climatology of the ORCA05-REF simulation. Here, leakage response is quasi-linear,
341 monotonously increasing with strengthening westerlies (Fig. 6b). This suggests that, with

342 a constant climatological representation of large-scale circulation, in particular that of the
343 Southern Ocean, the portion of the westerlies felt within AGIO's southern domain (35°S
344 – 48°S) does not cause a threshold in leakage response. Altering the boundary conditions
345 to that derived from the ORCA05-SHW+40% experiment (red cross in Fig. 6b),
346 effectively allows for an assessment of the influence a different Southern Ocean state
347 have on leakage. In this case, leakage behavior is similar to that of the two global models,
348 supporting the hypothesis that the threshold observed in leakage (Fig. 6b) originates from
349 the large-scale circulation.

350 4. Agulhas leakage transient response to increased 351 westerlies

352 For the purpose of exploring the time dependency of Agulhas leakage response to
353 increased westerlies, we focus on the SHW+40% case and expand the ORCA05
354 simulations to beyond the 10 years of common analysis. Fig. 7 shows the time evolution
355 of leakage and other parameters associated with the greater Agulhas system. Presented,
356 are the annual values beginning from model year 31, which is when the anomaly fields
357 are applied. Linear trends calculated from the reference experiment were removed from
358 all runs. Under background climatological forcing, these minor trends (between 0.1 %
359 and 2.5 % of the reference values per decade) represent the inherent numerical drift that
360 can reasonably be assumed to be similar in all simulations. The BASIN and LOCAL
361 decompositions are overlaid. Following a fast initial adjustment, three distinct stages in
362 leakage behavior in the ORCA05-SHW+40%-FULL case (red curve on Fig. 7) can be
363 noted; (i) A proportional increase (model year 34 – 47) followed by (ii) a rapid decline

364 (model year 47 – 50) and finally (*iii*) return to and decadal modulation around reference
365 values (beyond model year 50).

366 Stage-1: Lasting for about a decade, during Stage-1, the westerlies acting both
367 locally and outside the Agulhas region contribute towards increasing the leakage. This
368 produces an overall proportional response (40 % increase in winds resulting in ~40 %
369 increase in leakage), with a 1:3 ratio between LOCAL and BASIN. During Stage-1, the
370 mean value of leakage for the FULL experiment is significantly different at the 99 %
371 confidence level (Welch’s t-test) from the mean leakage value of the reference
372 experiment. As anticipated, no change is observed in the Agulhas Current, the Agulhas
373 Return Current (ARC) and Mozambique throughflow, since surface forcing is unchanged
374 equatorward of 35°S. The Antarctic Circumpolar Current (ACC) and south-west Indian
375 sub-gyre, during that period, adjust to the altered forcing, which thereafter determines the
376 timescale of the leakage response. Note that, we opt to measure the barotropic ACC
377 transport south of the African continent, the region that is most likely to impact the
378 Agulhas system. Qualitatively, there is little difference from measuring at other choke
379 points, at Drake Passage for example, where the reference value of ACC transport is
380 about 130 Sv, falling within observed ranges (Meredith et al. 2011).

381 Stage-2: Happening rapidly, within 4 model years (47 – 50), the decline appears
382 to occur indirectly as a result of the large-scale circulation adjustment. Without the large-
383 scale adjustment, a local increase in westerlies would maintain an increased leakage. The
384 decline coincides with the peak in ACC, the increase in ARC transport and variability,
385 and owing to the subtropical gyre spin-up, the increase in Mozambique throughflow. The
386 Agulhas Current also begins to respond accordingly.

387 Stage-3: Approximately 2 decades after the initial anomaly application, leakage
388 falls within the variability range of the reference experiment (with some decadal
389 variations around it). For Stage-3, the mean leakage value of the FULL experiment is
390 significantly not different at 99 % confidence level from the reference value. In response
391 to a 40 % increase in westerlies, the ACC stabilizes to ~20 % above reference (Fig. 7).
392 The strengthened sub-gyre results in the increase in Mozambique Channel flow (by ~25
393 %) and subsequent downstream increase of the Agulhas Current (by ~5 %). This Agulhas
394 Current transport increase occurs as an indirect effect of the westerlies increase. No
395 change in the East Madagascar Current transport is noted (not shown). The ARC speed
396 remains at an increased level (~23 % above reference values), with a ~60 % increase in
397 variance. Towards the end of the simulation (model year 90 onwards), due the increased
398 wind stress curl acting only over the southern portion of the subtropical gyres, the
399 stronger sub-gyre meridionally contracts and zonally widens. This is subsequently seen in
400 a slight reduction in Mozambique throughflow and Agulhas Current transport. The return
401 of leakage to reference values occurs due to the large-scale circulation, as suggested by
402 the BASIN experiment.

403 Fig. 8 shows the equivalent within INALT01. Comparing the two global models
404 provides a way of diagnosing the impact mesoscale activities of the wider Agulhas region
405 have on the leakage response. Perhaps surprisingly so, but as already seen in Fig. 6, the
406 general response to westerly winds increase is not altered. The adjustment happens
407 quicker, and Stage-3 is reached 2 – 3 years earlier. To test the impact of resolution on
408 domain decomposition, the LOCAL experiment (only decomposition falling entirely
409 within INALT01's nest boundaries) was repeated within INALT01. The response is as

410 anticipated similar (Figs. 6b and 8). The fact that the models agree in the response,
411 irrespective of resolution, points towards an underlying mechanism that is to some extent
412 resolution independent.

413 The response seems to be linked to the development of the ACC. In the Atlantic
414 sector of the Southern Ocean, an increase in westerlies promotes a spin-up of the Weddell
415 gyre and, due to an increased pressure gradient, also its expansion (not shown). This in
416 turn, leads to an overall increase in the width of the circumpolar current in the Atlantic.
417 Within the two global models, the dynamic front between the supergyre and the ACC
418 regime can be diagnosed from the zero barotropic stream-function line (see Fig. 3a).
419 During Stage-3, immediately south of the leakage corridor, this boundary migrates by $\sim 2^\circ$
420 equatorward.

421 In the Southern Ocean, resolving eddies is known to be important (Hallberg and
422 Gnanadesikan 2006; Böning et al. 2008; Spence et al. 2010). The ACC within INALT01
423 is represented at the same resolution as within ORCA05. Owing to the 2-way nesting
424 scheme adopted for INALT01 and the requirement for consistent comparisons across
425 models, the choice has been made not to parameterize eddies in ORCA05. However in
426 order to assess the dependence of the 3-stage response on firstly Southern Ocean eddies
427 and secondly on initial conditions, we repeated the ORCA05-REF and ORCA05-
428 SHW+40%-FULL experiments including the initial 20-year spin-up with parameterized
429 eddies (Gent and McWilliams 1990). Thickness diffusivities used are capped at 1000 m^2
430 s^{-1} but vary spatially and temporally, increasing with stratification and isopycnal slope.
431 These simulations showed the same 3-stage behavior in leakage response (including the

432 magnitude of the Stage-1 increase), with the only difference being a prolonged Stage-2
433 (figure not shown).

434 Seeking to confirm that the ACC generally influences Agulhas leakage, three
435 additional experiments were undertaken. In these experiments, the SHW+40% anomaly
436 field was further decomposed geographically and applied within ORCA05 (Fig. 4d-f).
437 Fig. 9 shows the general behavior in ACC-B and ACC-L following the same 3-stage
438 pattern as for FULL (Fig. 7). Within the given time frame, no response is seen when the
439 ACC-P decomposition is applied, potentially indicating that the westerlies acting over the
440 Pacific Ocean, Drake Passage and south of Australia, under this set-up, have no direct
441 immediate impact on leakage. A possible reason for this would be that the westerlies,
442 generally weaker in strength and lying about 5° poleward in the Pacific compared to the
443 Indian-Atlantic sector (Fig. 3), are not aligned to the core of the applied anomaly. The
444 response in ACC-B, similar in magnitude to that of FULL, suggests that the winds in the
445 region 18°W – 115°E, corresponding to the region of maximum climatological westerlies
446 (Fig. 3), sets the leakage response. Further confirming the ACC's influence, ACC-L, a
447 poleward extension of the LOCAL application, shows an initial increase of the same
448 magnitude as LOCAL and a subsequent 3-stage leakage response.

449 The time scale is set by the ACC. Following the ACC peak, both the leakage and
450 ARC (transport and variance) react with a decline and increase respectively (Figs. 7 – 9).
451 Averaging over two 5-year periods reveals that in Stage-1, the leakage increase is
452 coincidental with an increased eddy kinetic energy in the Cape Basin but a decrease in
453 the retroflexion region (Fig. 10a,c). Flowing adjoined and unidirectional to each other,
454 the interaction between the ACC and the ARC become important in Stage-3, where both

455 the retroflection and the ARC become more energetic and variable (Figs. 7 – 9, 10b,d).
456 This is characteristic of a turbulent retroflection regime (Le Bars et al. 2012). This
457 regime, which occurs at strong winds, leads to the increased volume transport (seen in
458 Stage-1 as increased leakage) to be lost through an enhanced interaction between the
459 ARC and the ACC.

460 5. Mechanism of leakage response to the westerlies

461 The region of positive wind stress curl in the South Indian and South Atlantic oceans
462 roughly lies between 15°S (maximum trades) and 50°S (maximum westerlies). The wind
463 stress curl yields negative Ekman vertical velocities (i.e. pumping) over this region,
464 which promotes an equatorward Sverdrup transport of the interior (Marshall and Plumb
465 2007). Fig. 11 schematically portrays the proposed mechanism of leakage response to
466 changes in the westerlies. Increasing the westerlies in the manner presented in this study
467 leads to an increased wind stress curl between the latitudes 35° and 50°S. The
468 equatorward interior flow across the southern portion of the supergyre is therefore
469 enhanced. In Fig. 11, this is depicted along 40°S, which roughly is the latitude of
470 separation between the westward flowing Agulhas leakage and the eastward flowing
471 Agulhas Return Current. By construction no change is applied to the winds at the
472 latitudes of the Agulhas Current, north of 35°S. Through continuity, the increased
473 meridional transport must result in a westward mass transport towards the South
474 America. Closing the circulation, the western boundary current subsequently increases.

475 Figs. 6b and 6c (gray lines) also show the change in theoretical meridional interior
476 flow (Sverdrup transport) along 40°S resulting from the added intensity anomalies. As
477 anticipated, the change in Sverdrup transport is a linear function of the change in wind

478 stress curl. Our results show that leakage change within the global models follows the
479 proportional Sverdrup transport change over the entire time-series for the reduced
480 westerlies cases (Fig 6b) and during Stage-1 of the intensified westerlies simulations
481 (Figs 7 and 8).

482 In the portrayal shown in Fig. 11, leakage corresponds to the westward flow south
483 of the African continent and is a passive component of the supergyre circulation. This has
484 three major implications. Firstly, it suggests that the process determining leakage would
485 be independent of retroflection energetics. In partial support for this, we showed that
486 eddy kinetic energy of the retroflection in Fig. 10 matches in sign with neither the initial
487 increase in leakage of Stage-1 nor the return to reference values in Stage-3. Eddy kinetic
488 energy of the retroflection is increased in Stage-3 compared to reference levels, while
489 leakage is unchanged. Therefore, there seems to be no link between the energetics of the
490 retroflection and the process behind leakage. Secondly, it backs up the conclusion of
491 Loveday et al. (submitted) who showed leakage to be decoupled from changes in the
492 Agulhas Current. During Stage-1, large response in leakage occurs without any change in
493 Agulhas Current. In Stage-3, the increase in Agulhas Current (an indirect consequence of
494 the westerlies increase) results in no change in leakage. Thirdly, as noted in Figs. 6 – 8,
495 the general pattern of leakage response to the westerlies change is reflected at all
496 resolutions; in other words, irrespective of the form of leakage. It is important to mention
497 here that we do not claim that leakage follows Sverdrup dynamics since non-linearity
498 plays a crucial role in determining the amount of water entering the South Atlantic. What
499 we noticed is that, given a change in the westerlies, leakage responds in the same way the
500 interior adjustment (described by the Sverdrup balanced) does.

501 Agulhas leakage response is transient (Figs 7 – 9). The time dependency is a
502 question of wave propagation, in particular internal planetary waves, similar to the
503 process that communicates the dynamical imprint of leakage across the South Atlantic
504 (van Sebille and van Leeuwen 2007, Biastoch et al. 2008b). Rossby waves set the
505 adjustment time of the ocean to large-scale forcing. The initial rapid oceanic adjustment
506 to the applied high-frequency wind forcing prior to Stage-1 (model years 31 – 33) is a
507 result of the fast propagation of barotropic Rossby waves, which establishes the Sverdrup
508 balance. Meanwhile, the westerly winds influence induces a baroclinic adjustment of the
509 eastward flowing ACC on decadal timescale. Additional controls, such as its width, its
510 variability and buoyant convection within and outside of the current further influence the
511 adjustment timescale of the ACC (Allison et al. 2011). The timing in Figs. 7 – 9 suggests
512 that the interaction between the ACC and the Agulhas system become important after 1 –
513 2 decades. The decrease in leakage in Stage-3 is preceded by an increasing variability of
514 the ARC, which occurs when the ACC reaches its peak. The precise mechanism behind
515 this interaction is beyond the scope of this study. Since both currents are unidirectional
516 and adjacent, meridional exchanges in lateral momentum and tracers between them may
517 be a likely explanation.

518 Thus far, we focused on the impact of westerlies intensity on the Agulhas system.
519 As noted earlier, idealized equatorward shifts of the westerly wind belt induces an
520 increase in leakage (Fig. 6a). This occurs as a result of the redistribution of momentum.
521 Our application of a northward shift of the westerlies strengthens the wind stress curl
522 between 35° and 45°S, while reducing it over the core of ACC (45° – 60°S). The overall
523 effect is similar to an increase in westerlies over the southern portion of the Indian Ocean

524 subtropical gyre which leads to an increase in leakage. In this case, leakage remains at a
525 constant increased level (persistent Stage-1) and a weaker ACC does not result in leakage
526 to be hampered. The opposite for poleward shifts also holds; reduced northward Sverdrup
527 transport across the southern boundary of the supergyre boundary leads to reduced
528 leakage. Towards the end of the SHW-4 simulation, there is an indication that the leakage
529 further decreases, exacerbated by an increased ACC which stimulates an enhanced
530 interaction with the retroflection and ARC. This, once again, is dynamically consistent as
531 described above.

532 6. Discussion

533 There is the common belief that a displacement of the zero wind stress curl line
534 equatorward (poleward) would narrow (widen) the gateway south of Africa allowing less
535 (more) leakage (Zahn, 2010). Our result shows the converse. Paleoceanographic
536 interpretations propose that, on centennial-millennial timescales, a displacement of the
537 subtropical front at the northern boundary of the ACC south of Africa, concomitant with
538 shifts and intensity changes in the westerlies, could be a major driver in modulating the
539 amount of leakage (Peeters et al. 2004; Bard and Rickaby 2009; Caley et al. 2012). In our
540 series of experiments, we observed no significant change in the latitudinal position of the
541 hydrographically-defined subtropical front (maximum temperature gradient) south of
542 Africa in response to changes in position of the zero wind stress curl line. However, we
543 cannot emphatically conclude that the front does not respond to westerly changes, since
544 we did not apply a corresponding thermohaline forcing. Our ocean/sea-ice only
545 simulations addressed the transient response of the Agulhas system. Processes such as
546 deep and bottom water formation, which indirectly respond to changing wind patterns,

547 would in the long term affect the hydrography of the Southern Ocean leading to possible
548 shifts of its fronts (Spence et al. 2010; Downes et al. 2011; Graham et al. 2012).

549 During the Last Glacial Maximum (~20 kyears ago), leakage reduction (Peeters et
550 al. 2004; Franzese et al. 2006), and possible ACC increase (Franzese et al. 2006; Otto-
551 Bliesner et al. 2006) with no change in retroflexion position (Franzese et al. 2009) have
552 been suggested. There is, however, large uncertainty regarding the state of the Southern
553 Hemisphere winds during glacial times (Kohfeld et al. 2013). To name but a few
554 examples of recent studies, Anderson et al. (2002) and Wyrwoll et al. (2000) reported an
555 intensifying poleward displacement of the westerly jet; Rojas et al. (2008) concluded a
556 decrease with no significant latitudinal shift while Toggweiler et al. (2006) deduced an
557 equatorward shift. It is therefore not possible, given the present limited knowledge of the
558 wind patterns of the Last Glacial Maximum, to confirm whether or not the dependency of
559 Agulhas leakage on the westerlies was dominant. Nonetheless, a leakage reduction
560 accompanied by a more vigorous ACC would be in line with our results.

561 Of current relevance, models simulate an increase in contemporary Agulhas
562 leakage (Biastoch et al. 2009b; Rouault et al. 2009). Biastoch et al (2009b) proposed that
563 a poleward shift in contemporary westerlies is responsible for this increase. Swart et al.
564 (2012) questioned the robustness of such a latitudinal shift in present-day westerlies in an
565 analysis of various coupled climate model products as well as observational reanalyzes
566 and found that instead significant strengthening of the westerlies rather than shift has
567 occurred. In the last 40 years, the westerlies have increased by about 25 % (Fig. 12). We
568 showed that leakage initially responds proportionally to increased westerlies (Stage-1 in
569 Figs. 7 and 8). In Fig. 12, this is reflected by the linear relationship for the SHW+20%

570 and SHW+40% cases. Note that Fig. 12 shows the area-averaged (20°W – 140°E, 35° –
571 65°S) change in westerlies and not the change in maximum zonal-averaged westerlies.
572 Also shown are decadal averages in leakage change derived from the hind-cast
573 experiments of ORCA05 and INALT01. Given the strong linear relationship ($r = 0.98$
574 and 0.96 for ORCA05 and INALT01 respectively), similar to that of the sensitivity
575 experiments, we can conclude that the upward trend in leakage reported by Biastoch et al.
576 (2009b) and Rouault et al. (2009) may reflect an unadjusted oceanic response to the
577 continuously increasing momentum input by the westerlies akin to Stage-1. We could
578 further speculate that, should the on-going wind change lessen or halt (Watson et al.
579 2012) in response to stratospheric ozone recovery (Son et al. 2010), future decadal trend
580 in leakage could weaken. This would naturally also depend on the timing and magnitude
581 of the ACC response. It is unclear whether or not the ACC is already eddy saturated
582 (Hallberg and Gnanadesikan 2006; Böning et al. 2008; Spence et al. 2010). We have
583 shown that the circumpolar current plays a relatively critical role in the transient 3-stage
584 leakage response. Therefore, should the ACC be weakly responsive (or unresponsive) to
585 the present-day increasing westerlies, a delay in the onset of a Stage-2-type leakage
586 response can be expected.

587 Rouault et al. (2009) and van Sebille et al. (2009) both related the strength of the
588 Agulhas Current with the magnitude of leakage. Within the present-day range of
589 transport values, they found a linear relationship between the two variables. They did,
590 however, disagree on the sign of that relationship. Results presented here suggest that
591 changes in leakage do not necessitate variations in upstream transport. The Agulhas
592 Current is influenced by both easterlies (Loveday et al. submitted) and westerlies (this

593 study, Stage-3), while leakage responds predominantly to the westerlies. The
594 disagreement between Rouault et al. (2009) and van Sebille et al. (2009) was most likely
595 an outcome of the different wind field products used in forcing their respective models.
596 In general, within an integral large-scale atmospheric system, statistical relationships
597 between the Agulhas Current and leakage do not necessarily imply cause and impact but
598 instead are manifestations of individual external forcing.

599 Resolution is an important aspect of Agulhas system modeling. The necessity to
600 resolve the Agulhas system adequately has been amply emphasized in the literature (e.g.
601 Biastoch and Krauss 1999; Biastoch et al. 2008c). Beal et al. (2011) even recommend
602 that at least a tenth degree horizontal resolution (e.g. INALT01) is required. Such
603 resolution has not yet been reached by most coupled climate models used for future
604 predictions (Taylor et al. 2012; Weijer et al. 2012). Here, while our series of experiments
605 demonstrate that leakage response to a constant change in westerly winds is represented
606 at all resolutions, we wish to stress the importance in considering the magnitude of the
607 response. For example, a 40 % increase in westerlies during Stage-1 results in
608 approximately the same percentage increase in leakage, which at low-resolution
609 (ORCA05) is ~10 Sv and at high-resolution (INALT01) is ~6 Sv. Coarse resolution
610 models clearly overestimate the actual volumetric transport and corresponding amount of
611 heat and salt exported into the Atlantic, which ultimately is of critical importance because
612 of the implications for the Atlantic meridional overturning circulation and global climate
613 (Biastoch et al. 2008b,c). Notwithstanding, within the $0.5^{\circ} - 0.1^{\circ}$ range, the mechanism
614 behind the response of leakage to changes in the westerlies is consistent.

615 Our study describes leakage response in the context of changes in the zonal
616 component of westerlies that are constant in time. In reality, the wind system changes
617 progressively and leakage is expected to respond non-linearly to the compounding effects
618 of migrations and magnitudes (deviation from linearity seen in Fig. 12). The meridional
619 component of the wind stress, albeit relatively small on average, may additionally play a
620 role which we have not considered here. Furthermore, changes in the transition zone
621 between the easterlies and westerlies (between 25° and 35°S) as well as the impact of
622 altered wind forcing on the thermohaline field may also be important.

623 7. Summary

624 We systematically deconstructed the manner in which the Southern Hemisphere
625 westerlies affect Agulhas leakage and reached the conclusion that the intensity of the
626 wind belt is predominantly responsible in controlling the Indian-Atlantic transport.
627 Agulhas leakage responds rapidly (within 2 – 3 years) and proportionally to changes in
628 the westerly wind stress. Change in leakage is comparable to the change in Sverdrup
629 transport across the southern portion of the supergyre. Shifts and modifications to the
630 intensity of the wind belt result in changes in wind energy input that, following Sverdrup
631 dynamics, cause an adjustment of the interior flow. South of Africa, that change is in turn
632 reflected as a change of leakage.

633 Simulations where the intensity of the westerlies was increased show a transient
634 response in leakage. Initially, leakage responds proportionally to the wind increase.
635 Subsequently, after 1 – 2 decades, leakage subsides to normal reference levels. The
636 transient response occurs due to the adjustment of the large-scale circulation. In

637 particular, energetic interactions between the Antarctic Circumpolar Current and the
638 Agulhas system cause the subsidence in leakage.

639 We also showed that the impact a displacement of the westerly wind belt has on
640 leakage can be regarded as a redistribution of momentum. Shifts of the westerlies
641 equatorward increase the energy input over the southern portion of the supergyre and
642 reduce it over the Southern Ocean. This results in enhanced leakage. Conversely,
643 poleward shifts reduces leakage and the reduction would be accentuated following the
644 adjustment (strengthening) of the circumpolar current. This result is at odds with previous
645 claims.

646 Our investigation further suggested that the process behind the leakage response
647 to changes in the westerlies is independent of model resolution, upstream transport of the
648 Agulhas Current and possibly retroreflection energetics. However, this does not discredit
649 the importance of non-linearity in the region. The volumetric change in leakage within
650 models is highly dependent on the correct representation of the numerous non-linear
651 interactions in the Agulhas system. More importantly, the corresponding changes in the
652 amount of heat and salt being exported have the potential of impacting the circulation in
653 the Atlantic.

654

655 *Acknowledgments.*

656 This work received funding from the European Community's Seventh Framework
657 Programme FP7/2007-2013-Marie-Curie ITN, under grant agreement 238512,
658 GATEWAYS project. Model experiments were performed at the High performance
659 computing centres in Stuttgart (HLRS) and in Cape Town (CHPC) as well as at the

660 Christian-Albrechts University of Kiel (NESH). The Ariane-v2.2.6 Lagrangian package
661 was used for Agulhas leakage calculation (<http://www.univ-brest.fr/lpo/ariane/>).
662 Altimetry data for model validation were downloaded from <http://aviso.oceanobs.com>.

663

664 **References**

665 Allison, L. C., H. L. Johnson, and D. P. Marshall, 2011: Spin-up and adjustment of the
666 Antarctic Circumpolar Current and global pycnocline. *J. Mar. Res.*, **69**, 167–189,
667 doi:10.1357/002224011798765330.

668 Anderson, R. F., Z. Chase, M. Q. Fleisher, and J. Sachs, 2002: The Southern Ocean's
669 biological pump during the Last Glacial Maximum. *Deep-Sea Res. II*, **49**, 1909–
670 1938, doi:10.1016/S0967-0645(02)00018-8.

671 Ansorge, I., S. Speich, J. R. E. Lutjeharms, G. J. Goni, C. J. de W. Rautenbach, P.
672 Froneman, M. Rouault, and S. L. Garzoli, 2005: Monitoring the oceanic flow
673 between Africa and Antarctica: Report of the first GoodHope cruise. *S. Afr. J.*
674 *Sci.*, **101**, 29–35.

675 Arakawa, A., and Y.-J. G. Hsu, 1990: Energy conserving and potential-ensrophy
676 dissipating schemes for the shallow water equations. *Mon. Wea. Rev.*, **118**, 1960–
677 1969.

678 Bard, E., and R. E. M. Rickaby, 2009: Migration of the subtropical front as a modulator
679 of glacial climate. *Nature*, **460**, 380–383, doi:10.1038/nature08189.

680 Barnier, B. and Coauthors, 2006: Impact of partial steps and momentum advection
681 schemes in a global ocean circulation model at eddy-permitting resolution. *Ocean*
682 *Dyn.*, **56**, 543–567, doi:10.1007/s10236-006-0082-1.

- 683 Beal, L. M., W. P. M. de Ruijter, A. Biastoch, R. Zahn, and SCOR/WCRP/IAPSO-
684 Working-Group-136, 2011: On the role of the Agulhas system in ocean
685 circulation and climate. *Nature*, **472**, 429–436, doi:10.1038/nature09983.
- 686 Biastoch, A., and W. Krauss, 1999: The Role of Mesoscale Eddies in the Source Regions
687 of the Agulhas Current. *J. Phys. Oceanogr.*, **29**, 2303–2317.
- 688 Biastoch, A., C. W. Böning, J. Getzlaff, J.-M. Molines, and G. Madec, 2008a: Causes of
689 Interannual–Decadal Variability in the Meridional Overturning Circulation of the
690 Midlatitude North Atlantic Ocean. *J. Climate*, **21**, 6599–6615,
691 doi:10.1175/2008JCLI2404.1.
- 692 Biastoch, A., C. W. Böning, and J. R. E. Lutjeharms, 2008b: Agulhas leakage dynamics
693 affects decadal variability in Atlantic overturning circulation. *Nature*, **456**, 489–
694 492, doi:10.1038/nature07426.
- 695 Biastoch, A., J. R. E. Lutjeharms, C. W. Böning, and M. Scheinert, 2008c: Mesoscale
696 perturbations control inter-ocean exchange south of Africa. *Geophys. Res. Lett.*,
697 **35**, L20602, doi:10.1029/2008GL035132.
- 698 Biastoch, A., C. W. Böning, F. U. Schwarzkopf, and J. R. E. Lutjeharms, 2009a: Increase
699 in Agulhas leakage due to poleward shift of Southern Hemisphere westerlies.
700 *Nature*, **462**, 495–498, doi:10.1038/nature08519.
- 701 Biastoch, A., L. M. Beal, J. R. E. Lutjeharms, and T. G. D. Casal, 2009b: Variability and
702 Coherence of the Agulhas Undercurrent in a High-Resolution Ocean General
703 Circulation Model. *J. Phys. Oceanogr.*, **39**, 2417–2435,
704 doi:10.1175/2009JPO4184.1.

- 705 Biastoch, A., and C. W. Böning, 2013: Anthropogenic Impact on Agulhas Leakage.
706 *Geophys. Res. Lett.*, **40**, 1–6, doi:10.1002/grl.50243.
- 707 Blanke, B., and P. Delecluse, 1993: Variability of the tropical Atlantic Ocean simulated
708 by a general circulation model with two different mixed-layer physics. *J. Phys.*
709 *Oceanogr.*, **23**, 1363–1388.
- 710 Boebel, O., J. Lutjeharms, C. Schmid, W. Zenk, T. Rossby, and C. Barron, 2003: The
711 Cape Cauldron: a regime of turbulent inter-ocean exchange. *Deep-Sea Res. II*, **50**,
712 57–86.
- 713 Böning, C. W., A. Dispert, M. Visbeck, S. R. Rintoul, and F. U. Schwarzkopf, 2008: The
714 response of the Antarctic Circumpolar Current to recent climate change. *Nature*
715 *Geosci.*, **1**, 864–869, doi:10.1038/ngeo362.
- 716 Caley, T., J. Giraudeau, B. Malaizé, L. Rossignol, and C. Pierre, 2012: Agulhas leakage
717 as a key process in the modes of Quaternary climate changes. *P. Natl. Acad. Sci.*
718 *USA*, **109**, 6835–6839, doi:10.1073/pnas.1115545109.
- 719 Chelton, D. B., R. A. DeSzoeki, M. G. Schlax, E. N. Karim, and S. Nicolas, 1998:
720 Geographical variability of the first baroclinic Rossby radius of deformation. *J.*
721 *Phys. Oceanogr.*, **28**, 433 – 460.
- 722 Cunningham, S. A., and R. Marsh, 2010: Observing and modeling changes in the Atlantic
723 MOC. *Wiley Interdisciplinary Reviews: Climate Change*, **1**, 180–191,
724 doi:10.1002/wcc.22.
- 725 de Ruijter, W. P. M., A. Biastoch, S. S. Drijfhout, J. R. E. Lutjeharms, R. P. Matano, T.
726 Pichevin, P. J. van Leeuwen, and W. Weijer, 1999: Indian-Atlantic interocean

- 727 Dynamics , estimation and impact ring shedding. *J. Geophys. Res.*, **104**, 20885 –
728 20910.
- 729 Debreu, L., and E. Blayo, 2008: Two-way embedding algorithms: a review. *Ocean Dyn.*,
730 **58**, 415–428, doi:10.1007/s10236-008-0150-9.
- 731 Dencausse, G., M. Arhan, and S. Speich, 2010: Spatio-temporal characteristics of the
732 Agulhas Current retroflection. *Deep-Sea Res. I*, **57**, 1392–1405,
733 doi:10.1016/j.dsr.2010.07.004.
- 734 Dijkstra, H. A., and W. P. M. de Ruijter, 2001: On the Physics of the Agulhas Current:
735 Steady Retroflection Regimes. *J. Phys. Oceanogr.*, **31**, 2971–2985.
- 736 Downes, S. M., a. S. Budnick, J. L. Sarmiento, and R. Farneti, 2011: Impacts of wind
737 stress on the Antarctic Circumpolar Current fronts and associated subduction.
738 *Geophys. Res. Lett.*, **38**, 3–8, doi:10.1029/2011GL047668.
- 739 Franzese, A., S. Hemming, S. Goldstein, and R. Anderson, 2006: Reduced Agulhas
740 Leakage during the Last Glacial Maximum inferred from an integrated
741 provenance and flux study. *Earth Planet. Sci. Lett.*, **250**, 72–88,
742 doi:10.1016/j.epsl.2006.07.002.
- 743 Franzese, A. M., S. R. Hemming, and S. L. Goldstein, 2009: Use of strontium isotopes in
744 detrital sediments to constrain the glacial position of the Agulhas Retroflection.
745 *Paleoceanography*, **24**, PA2217, doi:10.1029/2008PA001706.
- 746 Fyfe, J. C., and O. A. Saenko, 2006: Simulated changes in the extratropical Southern
747 Hemisphere winds and currents. *Geophys. Res. Lett.*, **33**, L06701,
748 doi:10.1029/2005GL025332.

- 749 Fyfe, J. C., O. A. Saenko, K. Zickfeld, M. Eby, and A. J. Weaver, 2007: The Role of
750 Poleward-Intensifying Winds on Southern Ocean Warming. *J. Climate*, **20**, 5391–
751 5400, doi:10.1175/2007JCLI1764.1.
- 752 Gent, P. R., and J. C. McWilliams, 1990: Isopycnal Mixing in Ocean Circulation Models.
753 *J. Phys. Oceanogr.*, **20**, 150–155.
- 754 Gordon, A. L., 1986: Interocean exchange of Thermocline Water. *J. Geophys. Res.*, **91**,
755 5037–5046, doi:10.1029/JC091iC04p05037.
- 756 Gordon, A. L., R. F. Weiss, W. M. Smethie, and M. J. Warner, 1992: Thermocline and
757 Intermediate Water Communication between the South Atlantic and Indian
758 Oceans. *J. Geophys. Res.*, **97**, 7223–7240.
- 759 Graham, R. M., A. M. de Boer, K. J. Heywood, M. R. Chapman, and D. P. Stevens,
760 2012: Southern Ocean fronts: Controlled by wind or topography? *J. Geophys.*
761 *Res.*, **117**, 1–14, doi:10.1029/2012JC007887.
- 762 Haidvogel, D. B., and A. Beckmann, 1999: *Numerical Ocean Circulation Modeling*.
763 Series on Environmental Science and Management: Volume 2, 344pp.
- 764 Hallberg, R., and A. Gnanadesikan, 2006: The Role of Eddies in Determining the
765 Structure and Response of the Wind-Driven Southern Hemisphere Overturning:
766 Results from the Modeling Eddies in the Southern Ocean (MESO) Project. *J.*
767 *Phys. Oceanogr.*, **36**, 2232–2252, doi:10.1175/JPO2980.1.
- 768 Hodgson, D. a., and L. C. Sime, 2010: Palaeoclimate: Southern westerlies and CO₂.
769 *Nature Geosci.*, **3**, 666–667, doi:10.1038/ngeo970.

- 770 Knorr, G., and G. Lohmann, 2003: Southern Ocean origin for the resumption of Atlantic
771 thermohaline circulation during deglaciation. *Nature*, **424**, 532–536,
772 doi:10.1038/nature01855.
- 773 Kohfeld, K.E., R. M. Graham, A. M. de Boer, L. C. Sime, E. W. Wolff, C. Le Quéré, and
774 L. Bopp, 2013: Southern Hemisphere westerly wind changes during the Last
775 Glacial Maximum: paleo-data synthesis. *Quat. Sci. Rev.*, **68**, 76–95,
776 doi:10.1016/j.quascirev.2013.01.017.
- 777 Large, W. G., J. C. McWilliams, and S. C. Doney, 1994: Oceanic vertical mixing: A
778 review and a model with a nonlocal boundary layer parameterization. *Rev.*
779 *Geophys.*, **32**, 363–403.
- 780 Large, W. G., and S. G. Yeager, 2009: The global climatology of an interannually
781 varying air–sea flux data set. *Climate Dyn.*, **33**, 341–364, doi:10.1007/s00382-
782 008-0441-3.
- 783 Le Bars, D., W. P. M. de Ruijter, and H. A. Dijkstra, 2012: A New Regime of the
784 Agulhas Current Retroflexion: Turbulent Choking of Indian–Atlantic leakage. *J.*
785 *Phys. Oceanogr.*, **42**, 1158–1172, doi:10.1175/JPO-D-11-0119.1.
- 786 Loveday, B. R., J. V. Durgadoo, C. J. C. Reason, A. Biastoch, and P. Penven, Decoupling
787 of the Agulhas Current from the Agulhas Leakage. *J. Phys. Oceanogr.*, submitted.
- 788 Madec, G., 2008: *NEMO ocean engine*. Note du Pole de modeisation de l’Institut Pierre-
789 Simon Laplace No 27, **ISSN No 12**, 215pp.
- 790 Madec, G., and M. Imbard, 1996: A global ocean mesh to overcome the North Pole
791 singularity. *Climate Dyn.*, **12**, 381–388, doi:10.1007/BF00211684.

- 792 Marchesiello, P., J. C. McWilliams, and A. Shchepetkin, 2001: Open boundary
793 conditions for long-term integration of regional oceanic models. *Ocean Modell.*,
794 **3**, 1–20, doi:10.1016/S1463-5003(00)00013-5.
- 795 Marchesiello, P., L. Debreu, and X. Couvelard, 2009: Spurious diapycnal mixing in
796 terrain-following coordinate models: The problem and a solution. *Ocean Modell.*,
797 **26**, 156–169, doi:10.1016/j.ocemod.2008.09.004.
- 798 Marshall, J., and R. Plumb, 2007: *Atmosphere, ocean and climate dynamics: an*
799 *introductory text*. Academic Press, 334pp.
- 800 Meredith, M. P. and Coauthors, 2011: Sustained monitoring of the Southern Ocean at
801 Drake Passage: Past achievements and future priorities. *Rev. Geophys.*, **49**,
802 RG4005, doi:10.1029/2010RG000348.
- 803 Oke, P., and M. England, 2004: Oceanic response to changes in the latitude of the
804 Southern Hemisphere subpolar westerly winds. *J. Climate*, **17**, 1040–1054.
- 805 Otto-Bliesner, B. L., E. C. Brady, G. Clauzet, R. Tomas, S. Levis, and Z. Kothavala,
806 2006: Last Glacial Maximum and Holocene Climate in CCSM3. *J. Climate*, **19**,
807 2526–2544, doi:10.1175/JCLI3748.1.
- 808 Ou, H., and W. de Ruijter, 1986: Separation of an inertial boundary current from a curved
809 coastline. *J. Phys. Oceanogr.*, **16**, 280–289.
- 810 Peeters, F. J. C., R. Acheson, G.-J. a Brummer, W. P. M. de Ruijter, R. R. Schneider, G.
811 M. Ganssen, E. Ufkes, and D. Kroon, 2004: Vigorous exchange between the
812 Indian and Atlantic oceans at the end of the past five glacial periods. *Nature*, **430**,
813 661–665, doi:10.1038/nature02785.

- 814 Penven, P., J. R. E. Lutjeharms, and P. Florenchie, 2006: Madagascar: A pacemaker for
815 the Agulhas Current system? *Geophys. Res. Lett.*, **33**, L17609,
816 doi:10.1029/2006GL026854.
- 817 Penven, P., P. Marchesiello, L. Debreu, and J. Lefèvre, 2008: Software tools for pre- and
818 post-processing of oceanic regional simulations. *Environ. Modell. Softw.*, **23**,
819 660–662, doi:10.1016/j.envsoft.2007.07.004.
- 820 Pichevin, T., D. Nof, and J. R. E. Lutjeharms, 1999: Why are there Agulhas Rings. *J.*
821 *Phys. Oceanogr.*, **29**, 693–707.
- 822 Richardson, P. L., 2007: Agulhas leakage into the Atlantic estimated with subsurface
823 floats and surface drifters. *Deep-Sea Res. I*, **54**, 1361–1389,
824 doi:10.1016/j.dsr.2007.04.010.
- 825 Ridgway, K. R., and J. R. Dunn, 2007: Observational evidence for a Southern
826 Hemisphere oceanic supergyre. *Geophys. Res. Lett.*, **34**, L13612,
827 doi:10.1029/2007GL030392.
- 828 Rojas, M. and Coauthors, 2008: The Southern Westerlies during the last glacial
829 maximum in PMIP2 simulations. *Climate Dyn.*, **32**, 525–548,
830 doi:10.1007/s00382-008-0421-7.
- 831 Rouault, M., P. Penven, and B. Pohl, 2009: Warming in the Agulhas Current system
832 since the 1980's. *Geophys. Res. Lett.*, **36**, L12602, doi:10.1029/2009GL037987.
- 833 Shchepetkin, A. F., and J. C. McWilliams, 1998: Quasi-monotone advection schemes
834 based on explicit locally adaptive dissipation. *Mon. Wea. Rev.*, **126**, 1542–1580.

- 835 Shchepetkin, A. F., and J. C. McWilliams, 2005: The regional oceanic modeling system
836 (ROMS): a split-explicit, free-surface, topography-following-coordinate oceanic
837 model. *Ocean Modell.*, **9**, 347–404, doi:10.1016/j.ocemod.2004.08.002.
- 838 Sijp, W. P., and M. H. England, 2008: The effect of a northward shift in the southern
839 hemisphere westerlies on the global ocean. *Prog. Oceanogr.*, **79**, 1–19,
840 doi:10.1016/j.pocean.2008.07.002.
- 841 Sijp, W. P., and M. H. England, 2009: Southern Hemisphere Westerly Wind Control over
842 the Ocean’s Thermohaline Circulation. *J. Climate*, **22**, 1277–1286,
843 doi:10.1175/2008JCLI2310.1.
- 844 Smagorinsky, J., 1963: General circulation experiments with the primitive equations. I.
845 The basic experiment. *Mon. Wea. Rev.*, **27**, 99–164.
- 846 Son, S.-W. and Coauthors, 2010: Impact of stratospheric ozone on Southern Hemisphere
847 circulation change: A multimodel assessment. *J. Geophys. Res.*, **115**, D00M07,
848 doi:10.1029/2010JD014271.
- 849 Speich, S., B. Blanke, and G. Madec, 2001: Warm and cold water routes of an OGCM
850 thermohaline conveyor belt. *Geophys. Res. Lett.*, **28**, 311–314.
- 851 Spence, P., J. C. Fyfe, A. Montenegro, and A. J. Weaver, 2010: Southern Ocean
852 Response to Strengthening Winds in an Eddy-Permitting Global Climate Model.
853 *J. Climate*, **23**, 5332–5343, doi:10.1175/2010JCLI3098.1.
- 854 Steele, M., R. Morfley, and W. Ermold, 2001: PHC: A global ocean hydrography with
855 high-quality Artic Ocean. *J. Climate*, **14**, 2079–2087.

- 856 Swart, N. C., and J. C. Fyfe, 2012: Observed and simulated changes in the Southern
857 Hemisphere surface westerly wind-stress. *Geophys. Res. Lett.*, **39**, 6–11,
858 doi:10.1029/2012GL052810.
- 859 Taylor, K. E., R. J. Stouffer, and G. A. Meehl, 2012: An Overview of CMIP5 and the
860 Experiment Design. *Bull. Amer. Meteor. Soc.*, **93**, 485–498, doi:10.1175/BAMS-
861 D-11-00094.1.
- 862 The DRAKKAR Group, 2007: Eddy-permitting ocean circulation hindcasts of past
863 decades. *CLIVAR Exchanges*, Vol. 12 of, 8–14.
- 864 Toggweiler, J. R., J. L. Russell, and S. R. Carson, 2006: Midlatitude westerlies,
865 atmospheric CO₂, and climate change during the ice ages. *Paleoceanography*,
866 **21**, 1–15, doi:10.1029/2005PA001154.
- 867 Tréguier A.-M., 1992: Kinetic energy analysis of an eddy resolving, primitive equation
868 North Atlantic model. *J. Geophys. Res.*, **97**, 687–701.
- 869 van Sebille, E., A. Biastoch, P. J. van Leeuwen, and W. P. M. de Ruijter, 2009: A weaker
870 Agulhas Current leads to more Agulhas leakage. *Geophys. Res. Lett.*, **36**, L03601,
871 doi:10.1029/2008GL036614.
- 872 van Sebille, E., and P. J. van Leeuwen, 2007: Fast northward energy transfer in the
873 Atlantic due to Agulhas rings. *J. Phys. Oceanogr.*, **37**, 2305–2315,
874 doi:10.1175/JPO3108.1.
- 875 van Sebille, E., P. J. van Leeuwen, A. Biastoch, and W. P. M. de Ruijter, 2010: Flux
876 comparison of Eulerian and Lagrangian estimates of Agulhas leakage: A case
877 study using a numerical model. *Deep-Sea Res. I*, **57**, 319–327,
878 doi:10.1016/j.dsr.2009.12.006.

- 879 Watson, P. a. G., D. J. Karoly, M. R. Allen, N. Faull, and D. S. Lee, 2012: Quantifying
880 uncertainty in future Southern Hemisphere circulation trends. *Geophys. Res. Lett.*,
881 **39**, L23708, doi:10.1029/2012GL054158.
- 882 Weijer, W. and Coauthors, 2012: The Southern Ocean and Its Climate in CCSM4. *J.*
883 *Climate*, **25**, 2652–2675, doi:10.1175/JCLI-D-11-00302.1.
- 884 Wyrwoll, K.-H., B. Dong, and P. Valdes, 2000: On the position of southern hemisphere
885 westerlies at the Last Glacial Maximum: an outline of AGCM simulation results
886 and evaluation of their implications. *Quat. Sci. Rev.*, **19**, 881–898,
887 doi:10.1016/S0277-3791(99)00047-5.
- 888 Zahn, R., J. R. E. Lutjeharms, A. Biastoch, G. Knorr, W. Park, C. J. C. Reason, 2010:
889 Investigating the Global Impacts of the Agulhas Current. *Eos. Trans. AGU*, **91**,
890 109-110.
- 891 Zalesak, S. T., 1979: Fully multidimensional flux corrected transport algorithms for
892 fluids. *J. Comput. Phys.*, **31**, 335–362.
- 893
- 894

895 **List of Figures**

896 FIG. 1. Mid-depth (250 – 400m) temperature (shading, °C) and velocity gradients (shown
 897 as the 3-dimentional-depth expression), 5-day average snapshot centered at 17 Jun 2006
 898 from the hind-cast realization of INALT01 illustrating the major pathway of Agulhas
 899 leakage across the South Atlantic. The INALT01 configuration consists of a global half-
 900 degree model with a tenth-degree nest over the region demarked by the grey box (50°S –
 901 8°N, 70°W – 70°E).

902

903 FIG. 2. Volume integrated (10°W – 60°E; 10° – 45°S) kinetic energy per unit mass ($\text{m}^2 \text{s}^{-2}$)
 904 with annual values (thick lines) overlaying monthly values (grey). Following a 20 year
 905 spin-up, reference (REF, black lines) experiments were performed for all three models.
 906 Wind anomalies were added from year 31; example of the SHW+40% (red lines) runs is
 907 shown. For the purpose of clarity, INALT01 values are offset by $1 \times 10^{20} \text{m}^2 \text{s}^{-2}$.

908 Common analysis period (model years 51 – 60) for Fig. 6 is indicated by the blue
 909 shading.

910

911 FIG. 3. (a) Wind stress magnitude (shading, N m^{-2}) and direction (vector) with horizontal
 912 barotropic stream-function contours overlay (data extracted from ORCA05-REF
 913 experiment); contour interval at 10 and 25 Sv for negative (dashed line) and positive (full
 914 lines) values respectively, thick contour represent the zero-line. (b) and (c) Zonally
 915 averaged (20° – 115°E) wind-stress (N m^{-2}) with thick black curve indicating the time-
 916 reference case. (b) Westerly position altered by -4° (blue), -2° (green), $+2^\circ$ (pink) and $+4^\circ$
 917 (red) about the mean (black), without changing the total energy input. (c) Intensity

918 change by -40 % (blue), -20 % (green), +20 % (pink), and +40 % (red) of the mean
 919 (black). Wind changes are applied within the region 35° – 63°S.

920

921 FIG. 4. Application of the SHW+40% anomaly (40 % intensification of westerlies). The
 922 wind stress anomaly (N m^{-2}) is applied (a) circumpolarly (FULL); (b) circumpolarly
 923 except the region bounded by 0° – 35°E, north of 45°S (BASIN); (c) only over the region
 924 bounded by 0° – 35°E, north of 45°S (LOCAL); (d) over region west of 18°E and east of
 925 115°E (ACC-P); (e) between region 18°W – 115°E (ACC-B); and (f) between region 0° –
 926 35°E (ACC-L).

927

928 FIG. 5. Representation of mean circulation (contours of sea surface height (SSH)
 929 averaged for period 1992 – 2007) and mesoscale variability (shading of SSH variance,
 930 cm^2) from (a) altimetric observation AVISO, (b) ORCA05, (c) AGIO and (d) INALT01.
 931 Sections used to measure Agulhas leakage across the Good-Hope Line (GH), the Agulhas
 932 Current (AC), the Mozambique throughflow (Moz) and the region where the Agulhas
 933 Return Current is monitored (box) are shown in (b). The domain used for the Lagrangian
 934 analysis is shown in (d).

935

936 FIG. 6. Change in Agulhas leakage (%) versus change in (a) position (°Lat) and (b & c)
 937 intensity (%) of the Southern Hemisphere westerlies (SHW). Reference values (black
 938 dot) are set at the origin for all three models and each dot represents a decade average
 939 (model years 51 – 60, blue shading in Fig. 2). (c) The decomposition between FULL,

940 BASIN and LOCAL is shown for the SHW-40% and SHW+40% cases. The gray line in
941 b & c represent the theoretical change in Sverdrup transport.

942

943 FIG. 7. Time-series for the REF and SHW+40% cases within ORCA05. Sections used to
944 measure the transports are shown in Fig. 5a and aside from the Agulhas leakage (AL), all
945 transports are measured from the barotropic stream-function: the Antarctic Circumpolar
946 Current (ACC) as the maximum stream-function south of Africa between 20° and 30°E;
947 the sub-gyre strength as the minimum stream-function value between 30° and 60°E; the
948 Agulhas Current (AC) as the minimum stream-function along the section at 32°S. For the
949 Agulhas Return Current (ARC), speed is for the top 1000 m. The light red, yellow and
950 blue shadings indicate Stage-1, Stage-2 and Stage-3 in ORCA05-SHW+40%-FULL
951 leakage response respectively (details in text).

952

953 FIG. 8. Same as Fig. 7 for INALT01.

954

955 FIG. 9. Time-series of Agulhas leakage (AL), Agulhas Return Current variance (ARC
956 Var) and Antarctic Circumpolar Current (ACC) transport from the ACC-P (pink), ACC-B
957 (blue) and ACC-L (green) decompositions of the SHW+40% anomaly within ORCA05.
958 The light red, yellow and blue shadings indicate Stage-1, Stage-2 and Stage-3 in
959 ORCA05-SHW+40%-FULL leakage response respectively (extracted from Fig. 7).

960

961 FIG. 10. Eddy Kinetic Energy (EKE) per unit mass anomaly at 100 m ($\text{cm}^2 \text{s}^{-2}$) within
962 ORCA05 (left) and INALT01 (right) averaged over model years 41 – 45 (a & c) and 56 –

963 60 (b & d). Contours indicate the respective averaged reference EKE values for model
964 years 41 - 60.

965

966 FIG. 11. Schematic of the proposed mechanism of leakage response to the westerlies.

967 Contours of barotropic stream function portray the anticyclonic supergyre (shaded area)

968 connecting the South Indian and South Atlantic oceans, with thick black contour

969 demarcating its boundaries (data extracted from ORCA05-REF experiment). Thick

970 arrows indicate the meridional Sverdrup interior flow and the corresponding zonal

971 transport that results from the wind stress application (REF in black and SHW+40% case

972 in red). The circulation is closed by the return flow of the western boundary currents

973 (dotted arrows).

974

975 FIG. 12. Change in Agulhas leakage (%) versus change in wind stress (%) averaged over

976 the region $20^{\circ}\text{W} - 140^{\circ}\text{E}$, $35^{\circ} - 65^{\circ}\text{S}$. Squares represent decadal averages from hind-cast

977 inter-annual (IA) simulations of ORCA05-IA (light blue) and INALT01-IA (light green),

978 with the period 1964-1973 taken as reference (set at origin); Circles represent Stage-1

979 averages (model years 41-45) from the FULL application of the SHW+20% and

980 SHW+40% anomalies as well as the corresponding REF (set at origin) within ORCA05

981 (blue) and INALT01 (green).

982 TABLE 1. Sensitivity experiments and their integration periods (in years). IA: Inter-
 983 Annual; REF: Reference; SHW: Southern Hemisphere westerlies. Domain
 984 decompositions are depicted in Fig. 4.

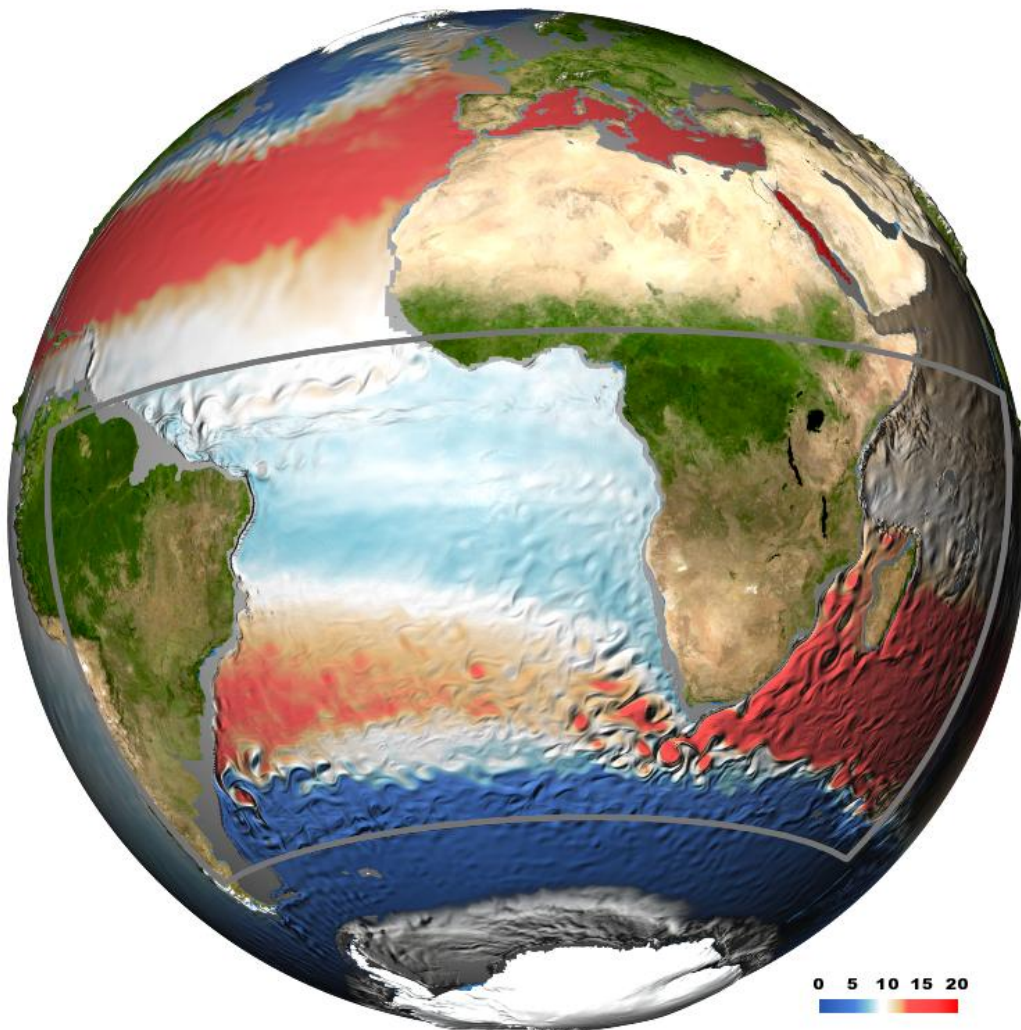
Experiment	Domain	Description	Model Configurations		
			ORCA05	AGIO	INALT01
IA	n/a	Inter-annual Reference	1948 – 2007		1948 – 2007
REF	n/a	Climatological Reference	1 – 110	1 – 60	1 – 60
SHW+4	FULL	4° Equatorward shift	31 – 60		31 – 60
SHW+2	FULL	2° Equatorward shift	31 – 60		
SHW-2	FULL	2° Poleward shift	31 – 60		31 – 60
SHW-4	FULL	4° Poleward shift	31 – 60		
SHW-40%	FULL	40 % Intensity decrease	31 – 110	31 – 60	31 – 60
	BASIN		31 – 60		
	LOCAL		31 – 60		
SHW-20%	FULL	20 % Intensity decrease	31 – 60	31 – 60	
SHW+20%	FULL	20 % Intensity increase	31 – 60	31 – 60	
SHW+40%	FULL	40 % Intensity increase	31 – 110	31 – 60	31 – 60
	BASIN		31 – 80		
	LOCAL				31 – 60
	ACC-P		31 – 60		
	ACC-B		31 – 60		
	ACC-L		31 – 60		
	ACC		AGIO boundary condition*	n/a	31 – 60

985 *Further details in text.

986

987

988

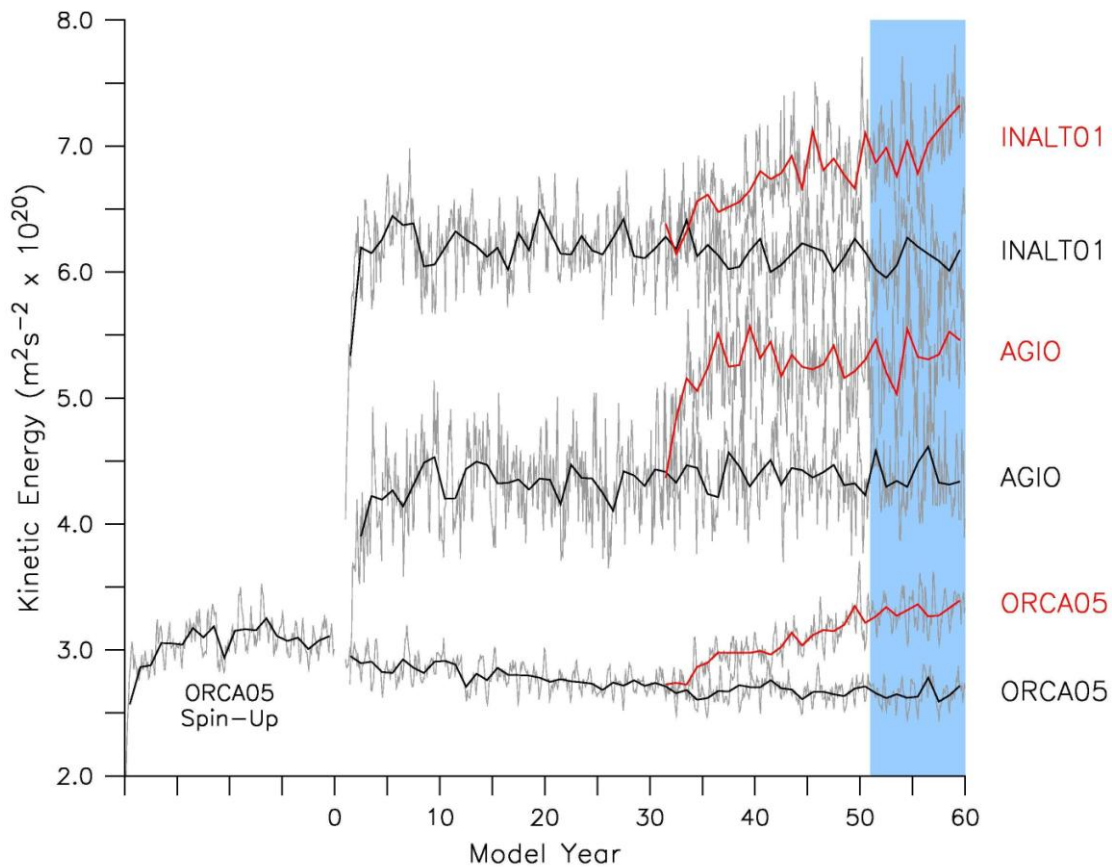


989

990 FIG. 1. Mid-depth (250 – 400m) temperature (shading, °C) and velocity gradients (shown
 991 as the 3-dimentional-depth expression), 5-day average snapshot centered at 17 Jun 2006
 992 from the hind-cast realization of INALT01 illustrating the major pathway of Agulhas
 993 leakage across the South Atlantic. The INALT01 configuration consists of a global half-
 994 degree model with a tenth-degree nest over the region demarked by the grey box (50°S –
 995 8°N, 70°W – 70°E).

996

997



998

999 FIG. 2. Volume integrated ($10^{\circ}\text{W} - 60^{\circ}\text{E}$; $10^{\circ} - 45^{\circ}\text{S}$) kinetic energy per unit mass ($\text{m}^2 \text{s}^{-2}$)1000 2) with annual values (thick lines) overlaying monthly values (grey). Following a 20 year

1001 spin-up, reference (REF, black lines) experiments were performed for all three models.

1002 Wind anomalies were added from year 31; example of the SHW+40% (red lines) runs is

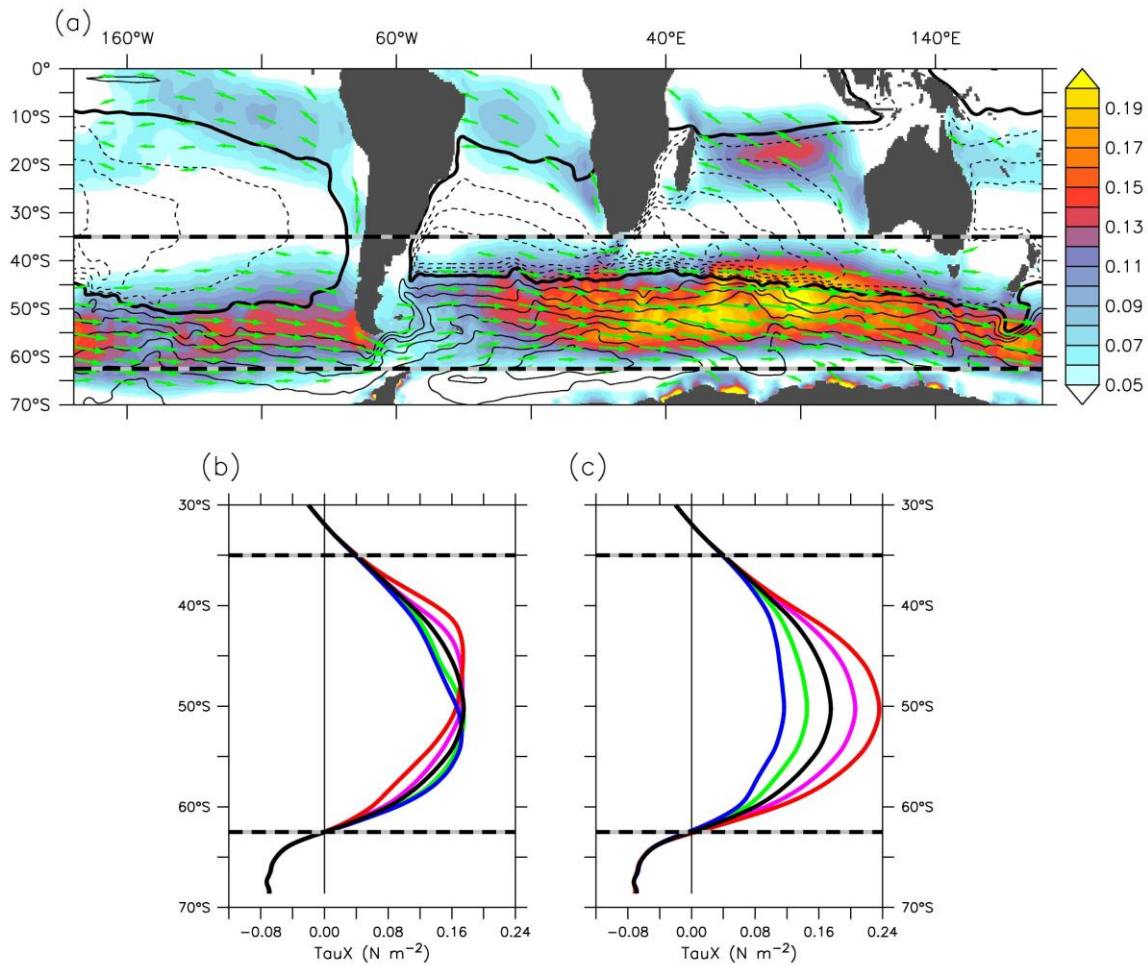
1003 shown. For the purpose of clarity, INALTO1 values are offset by $1 \times 10^{20} \text{ m}^2 \text{ s}^{-2}$.

1004 Common analysis period (model years 51 – 60) for Fig. 6 is indicated by the blue

1005 shading.

1006

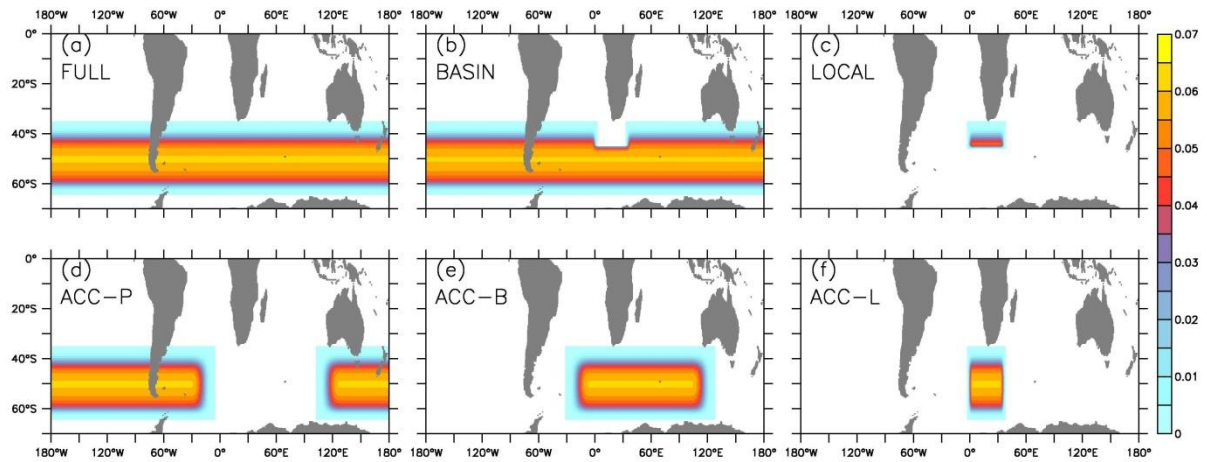
1007



1008

1009 FIG. 3. (a) Wind stress magnitude (shading, N m^{-2}) and direction (vector) with horizontal
 1010 barotropic stream-function contours overlay (data extracted from ORCA05-REF
 1011 experiment); contour interval at 10 and 25 Sv for negative (dashed line) and positive (full
 1012 lines) values respectively, thick contour represent the zero-line. (b) and (c) Zonally
 1013 averaged ($20^\circ - 115^\circ\text{E}$) wind-stress (N m^{-2}) with thick black curve indicating the time-
 1014 reference case. (b) Westerly position altered by -4° (blue), -2° (green), $+2^\circ$ (pink) and $+4^\circ$
 1015 (red) about the mean (black), without changing the total energy input. (c) Intensity
 1016 change by -40% (blue), -20% (green), $+20\%$ (pink), and $+40\%$ (red) of the mean
 1017 (black). Wind changes are applied within the region $35^\circ - 63^\circ\text{S}$.

1018



1019

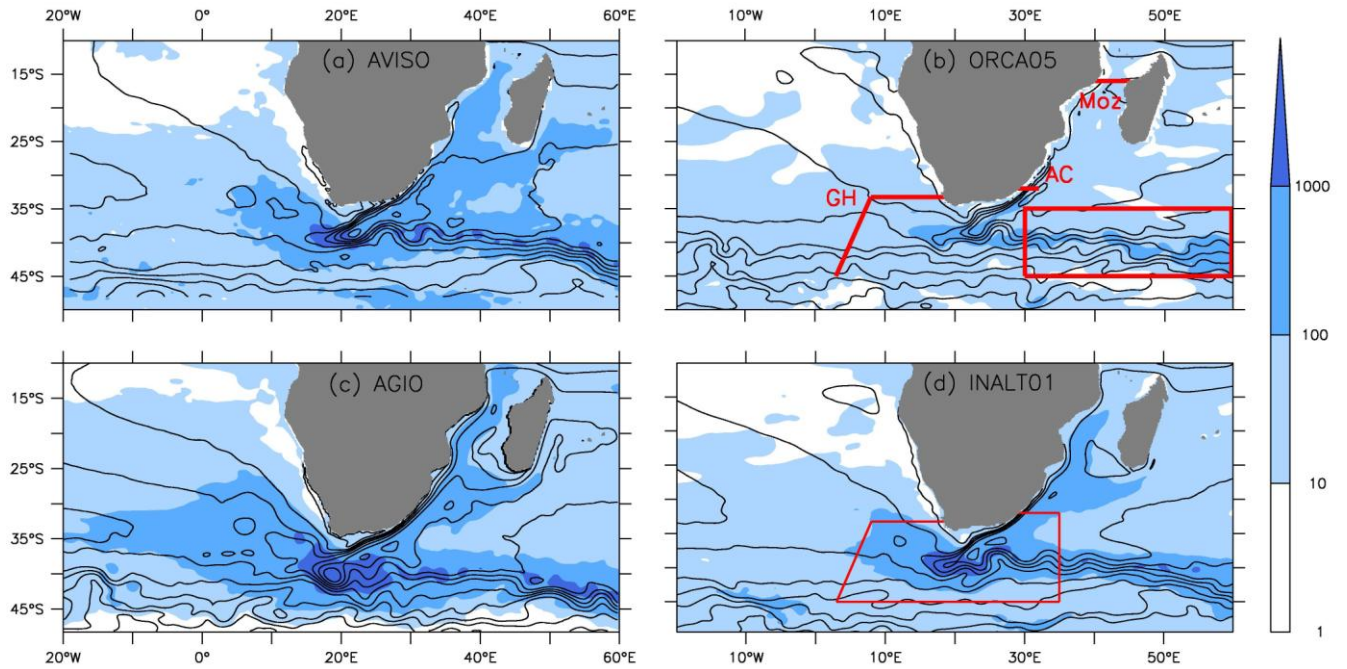
1020 FIG. 4. Application of the SHW+40% anomaly (40 % intensification of westerlies). The
 1021 wind stress anomaly (N m^{-2}) is applied (a) circumpolarly (FULL); (b) circumpolarly
 1022 except the region bounded by $0^\circ - 35^\circ\text{E}$, north of 45°S (BASIN); (c) only over the region
 1023 bounded by $0^\circ - 35^\circ\text{E}$, north of 45°S (LOCAL); (d) over region west of 18°E and east of
 1024 115°E (ACC-P); (e) between region $18^\circ\text{W} - 115^\circ\text{E}$ (ACC-B); and (f) between region $0^\circ -$
 1025 35°E (ACC-L).

1026

1027

1028

1029



1030

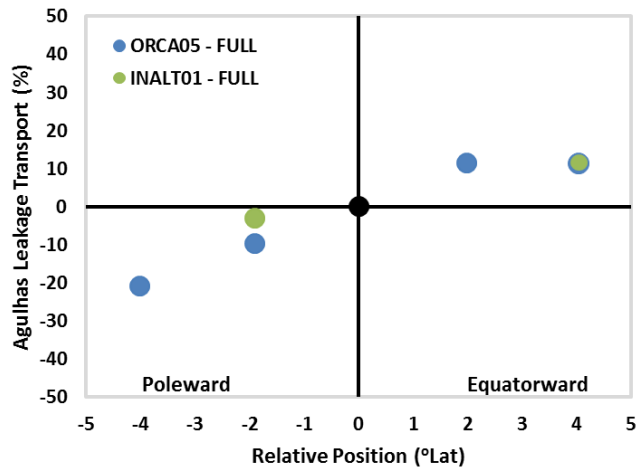
1031 FIG. 5. Representation of mean circulation (contours of sea surface height (SSH)
 1032 averaged for period 1992 – 2007) and mesoscale variability (shading of SSH variance,
 1033 cm^2) from (a) altimetric observation AVISO, (b) ORCA05, (c) AGIO and (d) INALT01.
 1034 Sections used to measure Agulhas leakage across the Good-Hope Line (GH), the Agulhas
 1035 Current (AC), the Mozambique throughflow (Moz) and the region where the Agulhas
 1036 Return Current is monitored (box) are shown in (b). The domain used for the Lagrangian
 1037 analysis is shown in (d).

1038

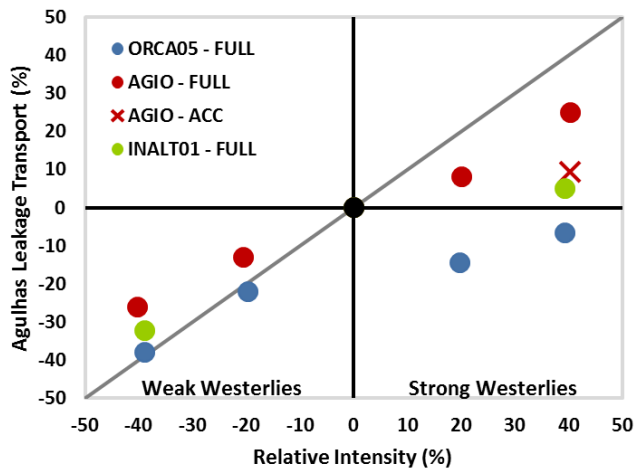
1039

1040

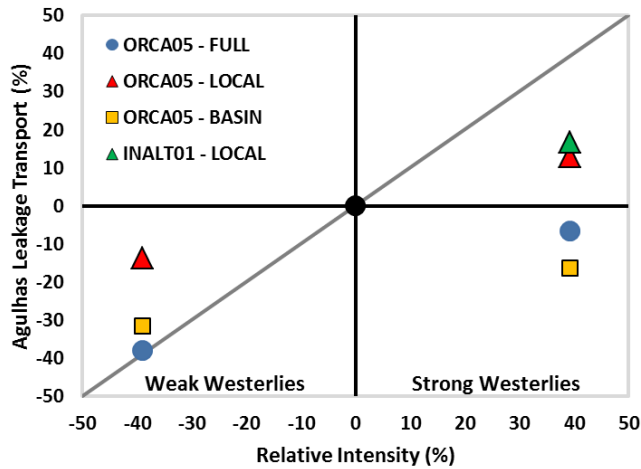
(a) SHW - Position



(b) SHW - Intensity



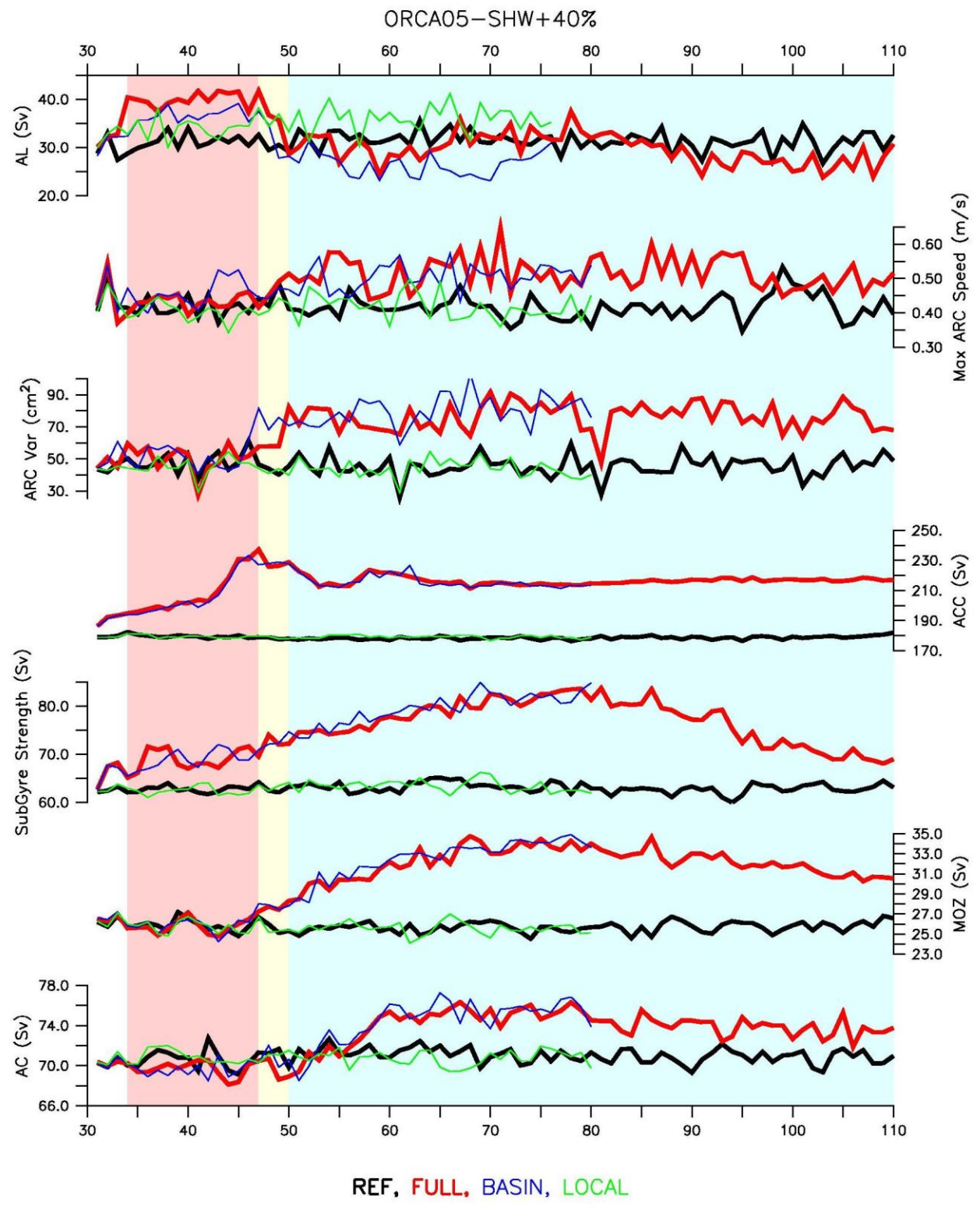
(c) SHW - Intensity Decomposition



1041

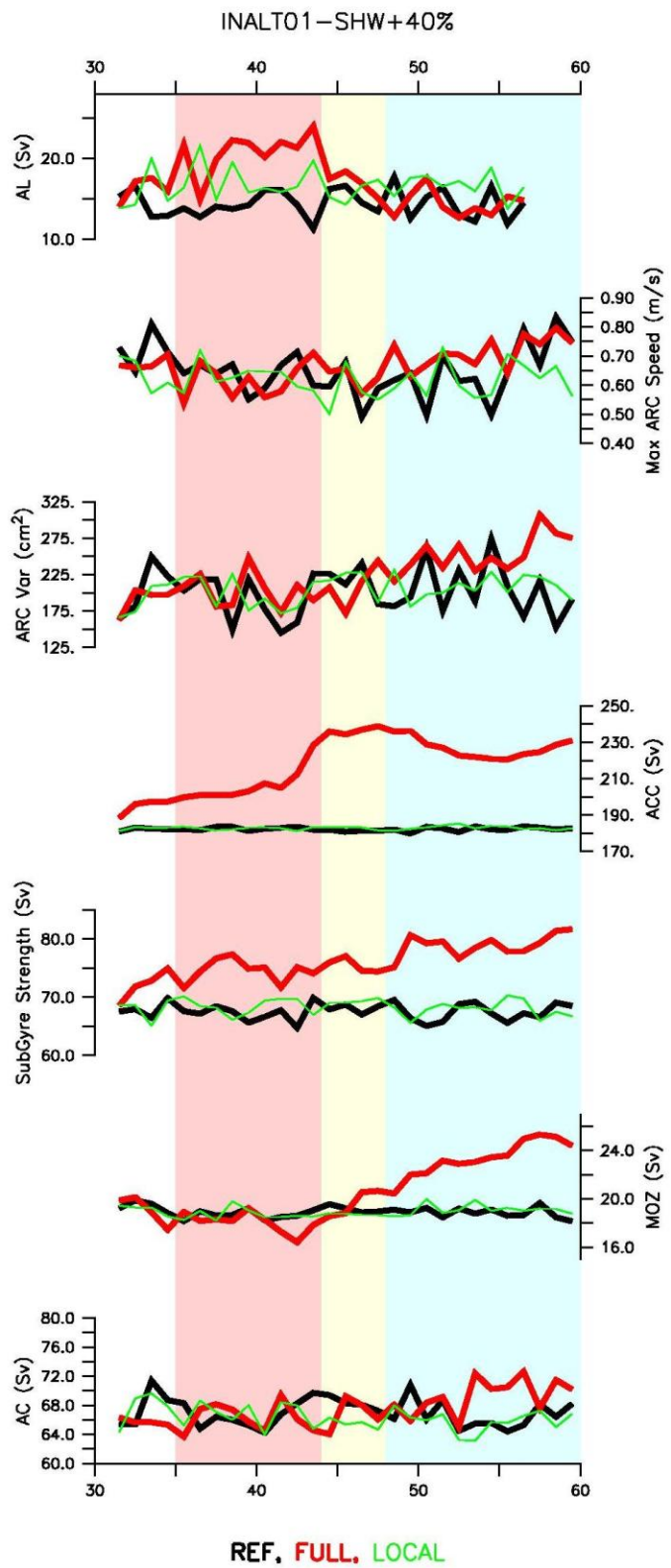
1042 FIG. 6. Change in Agulhas leakage (%) versus change in (a) position ($^{\circ}$ Lat) and (b & c)
1043 intensity (%) of the Southern Hemisphere westerlies (SHW). Reference values (black
1044 dot) are set at the origin for all three models and each dot represents a decade average
1045 (model years 51 – 60, blue shading in Fig. 2). (c) The decomposition between FULL,
1046 BASIN and LOCAL is shown for the SHW-40% and SHW+40% cases. The gray line in
1047 b & c represent the theoretical change in Sverdrup transport.
1048
1049

1050



1051

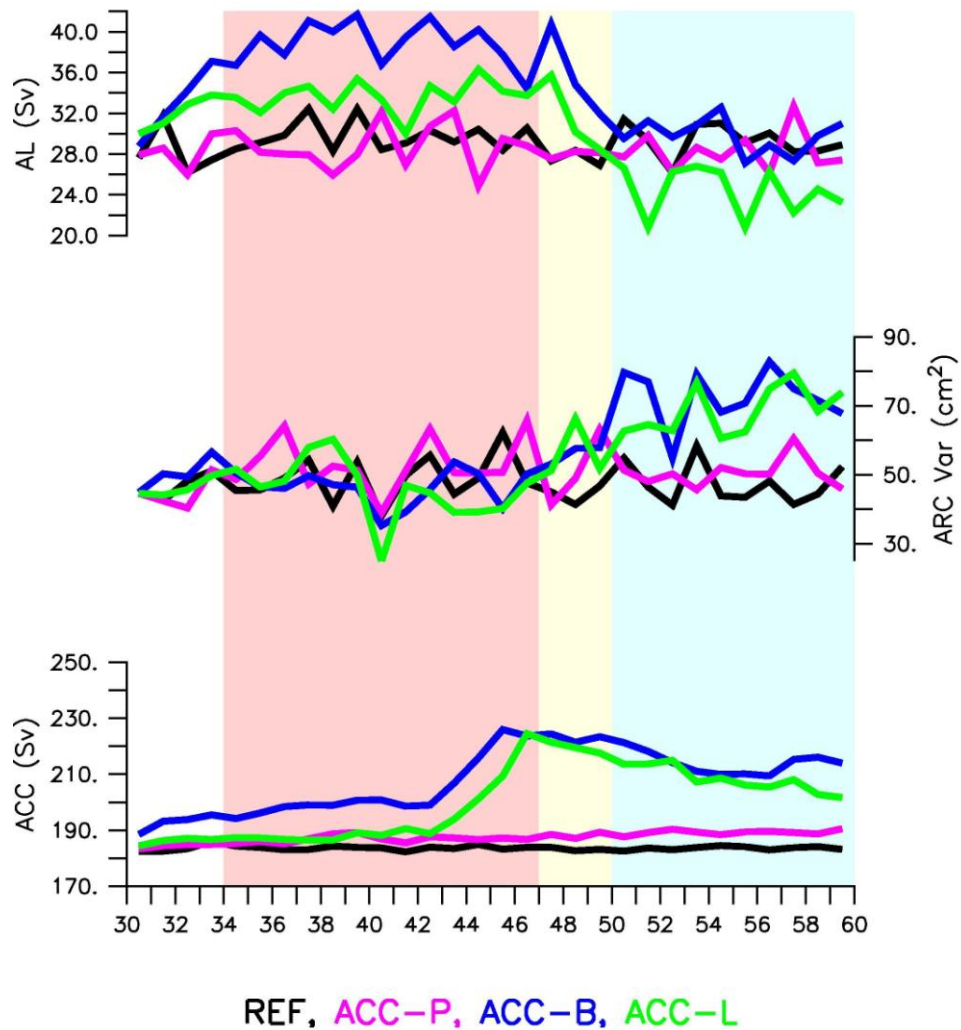
1052 FIG. 7. Time-series for the REF and SHW+40% cases within ORCA05. Sections used to
1053 measure the transports are shown in Fig. 5a and aside from the Agulhas leakage (AL), all
1054 transports are measured from the barotropic stream-function: the Antarctic Circumpolar
1055 Current (ACC) as the maximum stream-function south of Africa between 20° and 30°E;
1056 the sub-gyre strength as the minimum stream-function value between 30° and 60°E; the
1057 Agulhas Current (AC) as the minimum stream-function along the section at 32°S. For the
1058 Agulhas Return Current (ARC), speed is for the top 1000 m. The light red, yellow and
1059 blue shadings indicate Stage-1, Stage-2 and Stage-3 in ORCA05-SHW+40%-FULL
1060 leakage response respectively (details in text).
1061



1062

1063 FIG. 8. Same as Fig. 7 for INALTO1.

1064



1065

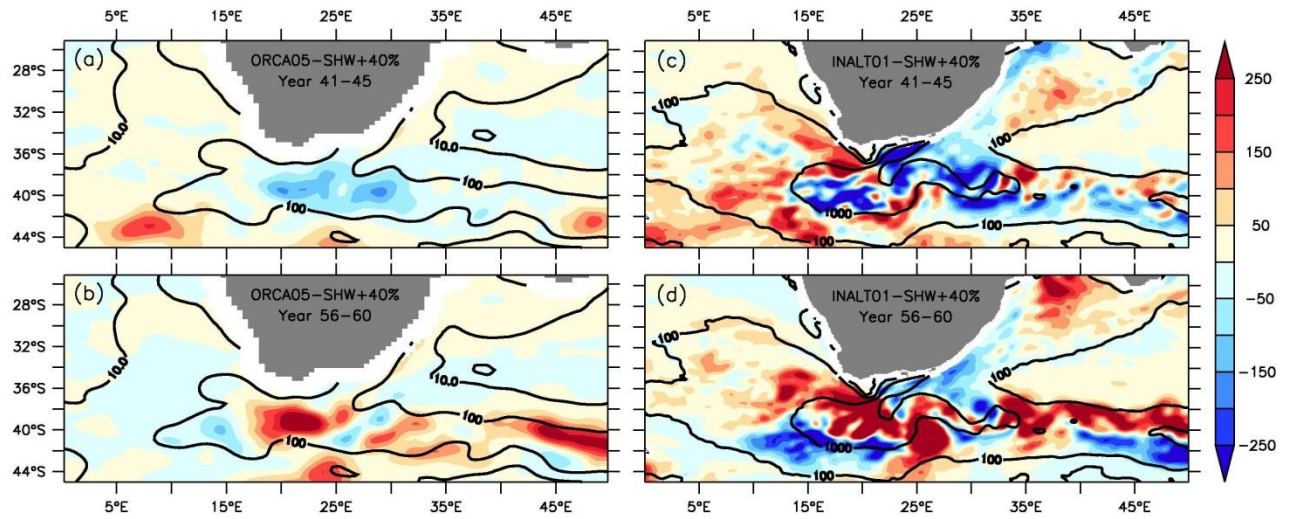
1066 FIG. 9. Time-series of Agulhas leakage (AL), Agulhas Return Current variance (ARC
 1067 Var) and Antarctic Circumpolar Current (ACC) transport from the ACC-P (pink), ACC-B
 1068 (blue) and ACC-L (green) decompositions of the SHW+40% anomaly within ORCA05.
 1069 The light red, yellow and blue shadings indicate Stage-1, Stage-2 and Stage-3 in
 1070 ORCA05-SHW+40%-FULL leakage response respectively (extracted from Fig. 7).

1071

1072

1073

1074

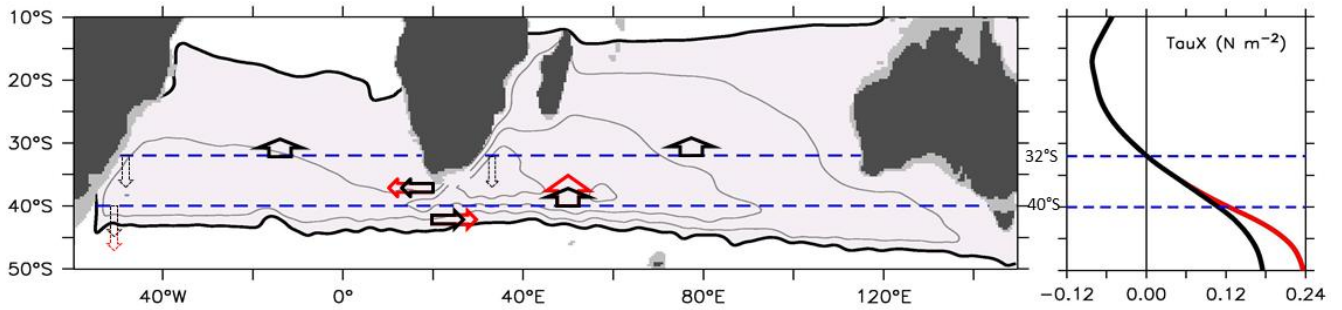


1075

1076 FIG. 10. Eddy Kinetic Energy (EKE) per unit mass anomaly at 100 m ($\text{cm}^2 \text{s}^{-2}$) within
 1077 ORCA05 (left) and INALT01 (right) averaged over model years 41 – 45 (a & c) and 56 –
 1078 60 (b & d). Contours indicate the respective averaged reference EKE values for model
 1079 years 41 - 60.

1080

1081



1082

1083 FIG. 11. Schematic of the proposed mechanism of leakage response to the westerlies.

1084 Contours of barotropic stream function portray the anticyclonic supergyre (shaded area)

1085 connecting the South Indian and South Atlantic oceans, with thick black contour

1086 demarcating its boundaries (data extracted from ORCA05-REF experiment). Thick

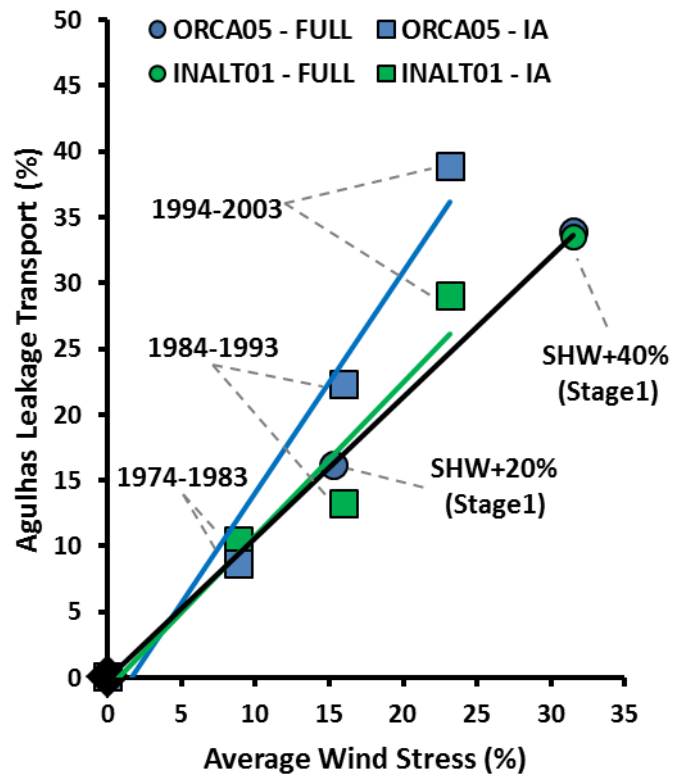
1087 arrows indicate the meridional Sverdrup interior flow and the corresponding zonal

1088 transport that results from the wind stress application (REF in black and SHW+40% case

1089 in red). The circulation is closed by the return flow of the western boundary currents

1090 (dotted arrows).

1091



1092

1093 FIG. 12. Change in Agulhas leakage (%) versus change in wind stress (%) averaged over
 1094 the region 20°W – 140°E, 35° - 65°S. Squares represent decadal averages from hind-cast
 1095 inter-annual (IA) simulations of ORCA05-IA (light blue) and INALT01-IA (light green),
 1096 with the period 1964-1973 taken as reference (set at origin); Circles represent Stage-1
 1097 averages (model years 41-45) from the FULL application of the SHW+20% and
 1098 SHW+40% anomalies as well as the corresponding REF (set at origin) within ORCA05
 1099 (blue) and INALT01 (green).

1100